Texture Encoded Realistic Joint Limits

David Kelly, B.Sc (DLIADT)

A dissertation submitted to the University of Dublin,
in partial fulfilment of the requirements for the degree of
Master of Science in Interactive Entertainment Technology

2008

Declaration

I declare that the work described in this document is, except where otherwise stated, entirely my own work and has not been submitted as an exercise for a degree at this or any other university.

Signed: _____ 10/09/2008

David Kelly, B.Sc (DLIADT)

Permission to lend and/or copy

I agree that Trinity College Library may lend or copy this dissertation upon request.

Signed: _____ 10/09/2008

David Kelly, B.Sc (DLIADT)

Acknowledgements

Thanks to my supervisor Ladislav Kavan for his advice and guidance throughout this project.

Thanks also to my class mates in Interactive Entertainment Technology whose friendship made the year most enjoyable.

Finally I wish to acknowledge my partner Sarah and for her support and understanding.

"The world of reality has its limits; the world of imagination is boundless."

Jean-Jacques Rousseau

Abstract

The motions achieved by virtual characters should satisfy anatomic constraints. Joint coupling and other concerns to this aim are often overlooked in existing research. The benefits of parameterisation of joint limits to a texture format in creation of a more complete system have been ill explored in existing research. I propose extensions to existing methods of limiting joint motion through the texture encoding of joint limits. It is the intent of this research to address the lack of suitable tools in the public domain for the editing and generation of complex joint limits in particular for use in video game applications.

Findings indicate that the proposed system is a highly efficient means to evaluate joint limits as it leverages the processing power of the GPU. Many of the desirable features for a joint limit system are addressed in this research and so is deemed a promising technique.

Table of Contents

Illustrative Material

Abbreviations

1-D, 2-D, 3-D	One, Two and Three Dimensions
AI	Artificial Intelligence
CPU	Central Processing Unit
CG	Computer Generated
DOF	Degrees of Freedom
FPS	Frames Per Second
GPU	Graphics Processing Unit
GUI	Graphical User Interface
HLSL	High Level Shading Language
IK	Inverse Kinematics
KB	Kilobyte
LEDs	Light emitting diodes
MB	Megabyte
RGB(A)	Red, Green, Blue & (Alpha)
R^3	Three dimensional space
R^4	Four dimensional space
S^3	3-sphere or hypersphere, is a higher-dimensional analogue of a sphere
SLERP	Spherical Linear Interpolation
UI	User Interface

Research Question

Is the use of a texture a suitable means for encoding rotational joint limits to meet the requirements of an advanced joint limiting tool?

Dissertation Roadmap

Literature Review

This chapter I discuss current solutions to joint limiting. Particular attention is paid to the feature set of existing tools utilising each method.

Artefact Design and Implementation

This chapter describes the avenues explored in creation of an artefact to address the research question.

Findings and Discussion

This chapter presents the results of data analysis and how these relate to the research question.

Recommendations for Further Work

In this chapter I explore the possibilities for further research.

Conclusion

This final chapter draws conclusions about the research questions supported by the findings from the data analysis.

Introduction

The geometric detail with which computer generated (CG) characters can be created has increased greatly in recent years. It has been noted that as the visual fidelity becomes more realistic the sensitivity of the viewer to discrepancies in the motion become more critical in creating a convincing scene (Hodgins, O'Brien, & Tumblin, 1998) and so more accurate articulation becomes key. This is especially relevant in simulations where perceived athleticism is tied to the coordination of movement of detailed polygonal characters as seen in modern video games (Shao & Ng-Thow-Hing, 2003).

What are joints?

In computer animation and biomechanical simulation, hierarchical structures of connected segments analogous to a human skeletal system are often used to articulate characters. The hierarchical structure is referred to as the *armature* or *skeleton* and the segments *bones*. *Joints* of varying degrees of required freedom (DOF) of movement form the connection between bones. Each bone in an armature has a local co-ordinate system associated with it. Rotation at the joint is defined with respect to the three orthogonal axes of this co-ordinate system. This local co-ordinate system is updated when *parent* bones (bones higher up the armature hierarchy) are manipulated and this linkage is described as a parent child relationship. A simplification of the true anatomical joint to a ball-and-socket joint which has three rotational DOF is used extensively for modelling the hip and shoulder joints of human characters. For Joints such as the human ankle two DOF may be sufficient while the human knee is often reduced to one DOF creating in effect a simple hinge.

The simplification to three DOF when applied to the shoulder complex removes the consideration of the clavicle and scapula articulations (pg.55, Figure 43) but is considered sufficient in most applications. Similarly research in this area concerns itself mostly with simplified purely rotational models. While the translation component of joint articulation is not profound in human joints, a more accurate modelling of the biology such as in (Lee & Terzopoulos, 2008) serves to better address it and other concerns.

Figure 1: Mechanical visualisation of various joints.

1-DOF Revolute joint	2-DOF Saddle Joint	3-DOF Ball-and-Socket Joint
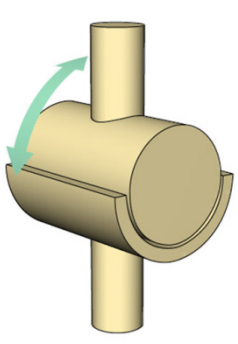	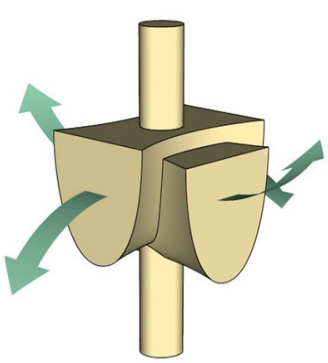	
Suitable for finger or knee	**Suitable for the wrist**	**Suitable for shoulder or hip**

What are joint limits?

Without restriction the three DOF of a virtual ball-and-socket joint can facilitate infinite spinning on the longitudinal axis and the directional vector component referred to as swing can sweep the surface of a sphere. As indicated such motion is only possible in a virtual world as any physical joint has mechanical impediments and so for realistic motion any representation of a joint should respect the permissible motion of said joint.

However parameterisation of the limits of the motion for a complex joint such as the shoulder is not an easy task. In humans not only does the physical topology of the joint restrict motion but also the muscular and ligament configuration is a factor. Finally collisions between body parts and the coupling of joints also restrict motion. A character armature without joint limits could achieve many unnatural postures. The resolving of joint limits is of use to an animator in the posing of a character for key frame animation. More importantly it is of significant use in higher level animation techniques such as procedural and artificial intelligence (AI) generated animation as well as kinematics, rag-doll physics simulations, the resolving of monocular motion capture and in full physics simulations such as for virtual occupants for car crash tests. Joint limits may also be of assistance to (or certainly contribute to a more convincing articulation when combined with) skin deformation techniques such as seen in (Kavan, 2008) and muscular deformation as seen in (Aubel & Thalmann, 2000).

Current dynamics techniques such as in (Wrotek, Jenkins, & McGuire, 2006) often do not explicitly respect joint limits but rather tend toward poses previously generated from motion capture. As AI control progresses towards generating motions without a motion capture base, such limitations will need to be addressed. The shoulder is widely regarded as the most complex joint in the body as so is the focus of my research.

Rotational parameterisation and dependencies

The parameterisation of rotations is used to encode orientations of armature bones creating poses. The non-Euclidean nature of rotations presents significant problems in any attempt to parameterise them to a Euclidean space. Singularities being the major problem which are rotational configurations where the quantities involved become infinite or nondeterministic. As noted in (Grassia, 1998) numerical tools most often employed in graphics assume Euclidean parameterisation and so conversion from a parameterisation space more suited for describing rotations is often required. The following is a discussion on the merits and pitfalls of common rotation parameterisations. The joint limit techniques utilising them will be discussed later.

Fixed axis and Euler angles

The Euler angle representation also known as the Pitch-Roll-Yaw representation records the rotational values about three orthogonal axes. For a three-DOF joint such as the shoulder there exist dependencies between the X & Y axial rotation axis often referred to as *swing* and the permissible longitudinal *Z-axis* rotation referred to as *twist* that should be captured and

respected. In medical terms swing constitutes a combination of abduction/adduction in the coronal plane and flexion/extension in the sagital plane.

The expression of joint limits in terms of hard limits on individual rotation angles as in (Craig, 1989) do not approach anatomical correctness and so are unsatisfactory for realistic animation. Furthermore to parameterise using the Euler angle representation presents the widely known singularity problem of gimbal lock. Creation of gimbal lock is dependent on the order of rotation about each axis. Gimbal Lock is the loss of control of one axis due to an alignment of axes resulting from calculation with respect to a fixed global axis or with Euler angles a 90^{o} rotation causing a loss of a degree of freedom. There exist twenty-four variations of Cartesian axis order for Euler angles (12x2 when considering if notation is fixed or rotating axes). This clearly complicates matters of communication and conversion with different fields interpreting a Euler angle expression (without explicit labelling of parameters) differently.

Never the less Euler angles are the most commonly used means of setting joint limits as their use enables a simple interface of three independent sliders for animator manipulation. While unsuitable for three DOF a Euler angle representation is considered suitable for a one DOF joint and in some circumstances a two DOF joint. Where the range of motion in terms of a single axis is not independent from the other axis (or axes) then Euler angles are not satisfactory. The conversion of Euler angles to a single rotation matrix typically involves the multiplication of three individual matrices (one for each rotational axis). The result as per matrix mathematics is dependent on the multiplication order. The conversion to axis–angle representation is not straight forward.

Rotational Matrices

A rotation matrix is created from multiplication of three 3x3 matrices, one for each axis with the order of multiplication being very important. The creation of each of the three matrices requires calculation of sine and cosine trigonometric functions. A format consisting of nine parameters is clearly not concise, however matrices are used extensively in graphics as higher dimensional matrices can perform not just rotations. Transformations such as scaling and translation are straightforward in matrix formulation.

Axis-angle

This representation consists of a unit vector representing an arbitrary axis of rotation, and θ a rotation about that vector. It is considered a highly intuitive rotation representation. Axial rotation is composed of rotation about the x-axis (abduction/adduction) and the y-axis (flexion/extension). Twist being the longitudinal rotation about the z-axis. While interpolation of the angle and axis can be conducted separately interpolation via axis-angle is less smooth in motion than a quaternion system. Another issue is that the resulting orientation of a rotation of zero degrees about any unit vector is equivalent and so an infinite number of solutions for that orientation exist.

Exponential Map

In this approach orientation is represented as a vector in R^3. But rather than the unit length vector of axis-angle exponential map uses a non-normalized vector. The direction of the vector is the axis to rotate about and the magnitude of the vector is the angular quantity to rotate by. The zero vector represents the identity rotation. Singularities are present but techniques for their avoidance are easily followed. Exponential maps have good interpolation behaviour as formulations permitting the conversion to and from S^3 (3-sphere) help in evaluating optimal interpolation.

Conversion to a quaternion is a similar formula to that required for the axis-angle conversion. The difference being exponential maps encode both magnitude and axis of a rotation into a single three-vector rather than a three-vector and an angle. A reordering of the axis-angle conversion formula ensures that instability incurred from the calculation of $\hat{v}$ ($\hat{v}$ being v/|v|) as |v| approaches zero is minimized.

Equation 1: Quaternion to exponential map conversion

$$\mathbf{q} = [q_x,q_y,q_z,q_w]^T = \left[\frac{\sin(½\theta)}{\theta}v,\ \cos(½\theta)\right]^T$$ *(where $\theta = |v|$)* (Grassia, 1998).

As with axis-angle singularities occur at rotations of multiples of 2π. Intuitively this is because a 360 degree rotation is the same as zero. "So if we can restrict our parameterisation to the inside of the ball of radius 2π we will avoid the singularity" (Grassia, 1998).

Quaternions

Discovered by Sir William Rowan Hamilton a quaternion **q** has four components q_x,q_y,q_z and q_w. We may parameterise a rotation of θ radians about the unit axis $\hat{v}$ R^3 with a unit quaternion constructed like so:

Equation 2: Quaternion from axis-angle conversion

$$\mathbf{q} = [q_x,q_y,q_z,q_w]^T = [\sin(½\theta)\ \hat{v},\ \cos(½\theta)]^T$$ (Grassia, 1998).

Any non zero quaternion can represent a rotation however unit quaternions are used for the ease of conversion from axis-angle formulation as shown above. For unit quaternions, the scalar component q_w can be deduced from the vectorial part q_x,q_y,q_z as follows:

Equation 3: Quaternion scalar component determination

$$q_w = \pm\sqrt{1.0 - q_{x^2} - q_{y^2} - q_{z^2}}$$

The above fact is exploited in the technique of Herda (Herda, Urtasun, & Fua, 2003) to be discussed later. Unit quaternions describe rotations and their subset of R^4 (four dimensional space) is referred to as S^3 which is a hyper-sphere. The extra dimension presented by unit quaternions embedded in R^4 ensures their freedom from singularities as the four partial

derivates exist and are linearly independent over all of S^3 (Grassia, 1998). Quaternions have other benefits such as the use of techniques which provide means to perform smooth interpolation of rotations. Respecting the unitary condition of quaternions presents a challenge that has been addressed in (Schmidt & Niemann, 2001) but adds computational complexity. Shoemake's (Shoemake, 1985) spherical linear interpolation curves (slerps) may show discontinuity at the joining keyframe between segments but more recent research (Ramamoorthi & Barr, 1997) has developed the generation of quaternion splines to minimize such energy.

The quaternion multiplication operator corresponds to matrix multiplication of rotation matrices. Conversion of a unit quaternion to a rotation matrix (matrix operations being the corner stone of the majority of graphics applications) is relatively simply and involves no trigonometric functions (which are considered to be performance bottlenecks in most execution architectures).

For all their uses however it could be argued that the adoption of quaternions has been slow paced with rotational matrices being more widely used in graphics applications.

Summary

The expression of rotations with quaternions as in Shoemake [Shoemake 1985] completely avoids singularities and has desirable interpolation properties. Exponential maps as presented by Grassia [Grassia 1998] can be configured to avoid singularities and have similar interpolation properties. Axis-angle singularities are also relatively easily avoided but interpolation is performed independently on the vectorial and angular components. Singularities are inherent and systemic with a Euler angle formulation and their interpolation is problematic.

Desired features for a joint limit system

The following is a list of properties that I believe to be of benefit to a joint limit system. I propose that a system satisfying of all of these requirements would be of significant use to future video game production.

Accuracy of result and a convenient means of limit storage

If a discretisation of the infinite vector and rotation combinations possible is required the format should have a determinable level of accuracy. Artificial limits such as a restriction of vector movement to a single hemisphere in contrary to anatomical limits as seen in (Engin & Tümer, 1989) should not be introduced. The means of storage for limits should enable processing in a straight forward fashion. To be able to intuit the limits from the storage format could be of benefit for conceptual understanding of the process. The format of storage should be scalable in its means of parameterisation enabling a greater or lesser accuracy where data size is of concern or is of use in the faster resolution of limits.

Need for variance from generic constraints

While (Wang, et al., 1998) show the variance in permitted joint motion between human subjects without any musculoskeletal abnormalities or history of joint trauma is negligible there may exist reasons not to use a single standard across all characters. Adjustment to joint limits should be possible to account for restrictions imposed by bulky clothing and equipment often seen in video game characters or other impediments to the natural range of motion. Some such extra restrictions could be accounted for through the augmentation of generic joint limits with polygon collision detection techniques. However the use of single system to control the range of motion would be desirable as any collision detection technique must cope with the growing polygonal complexity of computer generated characters. Also limits derived from a motion capture data set may not be sufficiently complete as recording all permissible motion in this manner is not without its challenges and repeated motion capture sessions for the purpose of filling data holes or correcting errors may be untenable. An interactive system that can be used to generate joints limits or generate divergences from generic recorded biomechanical values is so necessitated.

The generation and amending of joint limits within the three dimensional (3-D) space is perhaps more intuitive than 2-D based methods, though the required fine motion control in 3-D space presents an issue for most user interfaces (UIs). Methods such as spherical polygons would seem to bypass such interaction difficulties through the requirement of only a small number of key points for generation of swing boundaries. The level of detail in such boundaries may not be sufficient in all applications as discussed above. While no hard limit on the number of key points is set in the spherical polygon technique current tools for their generation do not present an intuitive solution to the interaction requirement. It is proposed that a course limit should be generated through manipulation of the joint in 3-D space through a suitable interface and where detailed refinement is required a 2-D system be employed.

Address tools issue

Research in the area of joint limits has been sporadic with the last paper of significance being (Herda, Urtasun, & Fua, 2005). In spite of this it is my belief that rather than a lack of applicable techniques the primarily impediment to the adoption of complex joint limits is the lack of a user friendly means for their use in commercial 3-D modelling packages. In terms of users the high-end of the 3-D modelling software market is dominated by Maya from Autodesk and XSI from Softimage. 3D Studio Max by Autodesk is likely the most used package in the middle to high range market. Blender is an open source program being actively developed by the Blender Foundation with a feature set comparable to that of 3D Studio Max. Blender is free to download however its penetration of the market is minimal in comparison to 3D Studio Max. This may in part be attributable to the ease with which illegal copies of commercial software can be obtained. The afore mentioned packages permit the creation of extensions to their feature set through scripts and plug-ins. However the ability to access the full source code for Blender made it the more obvious choice for development.

The system being proposed aims to combine the benefits of existing techniques while keeping the conceptual complexity to a minimum in its use as a tool. Its embedment in the free Blender 3-D package has been prototyped and it is hoped this move will remove barriers to the techniques' adoption.

As seen in (pg. 56, Figure 46, Figure 47, Figure 49 and Figure 50) the setting of Min/Max parameters along the local X, Y, and Z axes of a bone is the usual means for setting rotational limits in 3-D suites. These parameters are variously set by sliders, angle entry into text boxes or more direct interaction with the bone on each axis. As already discussed the limits generated from individual Euler angle systems are insufficient for the modelling of complex joints.

More advanced tools for the manipulation and storage of complex rotational joint limits in an intuitive manner are not common in video game asset production pipelines (Shao & Ng-Thow-Hing, 2003) or to my knowledge in other related fields. The above mentioned lack of tools suited for use by animators has necessitated manually key framed animation in the majority of applications.

Joint Coupling

For certain shoulder rotations there is a limit on the amount of permissible elbow flexion due to the presence of the head and thorax. Similar such constraints exist for the coupling of hip and knee joints. Such dependencies are often not addressed in existing research. Where addressed such as in (Herda, Urtasun, & Fua, 2005) the complexity of the solution is perhaps a deterrent to its implementation in video games.

Limit avoidance and stress measurement

Humans experience differing levels of resistance and physical discomfort when approaching the true limits of their joint motion. Given that some motions may be undesirable for a human performer for the above reason, it would be desirable for any AI controlled or generated motion to consider this. The issue of how to encode a varying preference to remain away from joint limits or the degree to which limits can be exceeded before a change in simulation is required such as bone breakage is ill explored in current research.

Requirement for real-time evaluation and resolution of limits

For real-time applications the resolution of joint constraints should not be computationally expensive. In particular many existing techniques try to reduce or avoid completely the use of trigonometric functions, which are known to be computationally expensive.

Fixed execution for limit test and limit resolution

Video games aim to have a fixed execution time per game tick allowing time for the required graphical frames per second (FPS) to be achieved. Any joint limiting and joint resolution algorithm will be given a fixed portion of the game tick budget in which to execute. The algorithm should therefore ideally complete within this allocation. However the required size of this allocation is difficult to calculate for algorithms that return results after a varying amount of processing. In such instances to ensure completion per game cycle the worst case processing time would need to be budgeted for. The budget may not stretch or for results returned within the budget a sleep may be necessitated for an even frame rate.

Where variable calculation times are unavoidable it is proposed that algorithms should be capable of returning their best guess once their budget is approached rather than exceeding it.

Achieving interactive frame rates for a large number of characters simultaneously poses challenges for many existing methods due to computational load. Gaming trends would seem to suggest this issue needs to be addressed as such future games may attempt to approach dynamic scenes in the order of complexity seen in the “Lord of the Rings” film battles. Games such as “Heavenly Sword” by Ninja Theory and “Dead Rising” by Capcom are already showing many hundreds of interactive characters on screen though their motion is largely key frame based. A deterministic execution for both limit testing and beyond limit resolution would be desirable for scheduling in resource hungry environments such as video game execution cycles.

State-of-the-art of joint limit data collection

The following research is concerned with the generation or collection of joint limit data. It is desirable that joint limits be as true to reality as possible. For this reason the direct recording from a human subject would be advantageous to correlate with empirical observations.

Non optical means

Goniometers

In occupational therapy and physical therapy, a device known as a goniometer is used in the assessment of patient range of motion. Through use of multiple such devices it is conservable that the dependencies of permissible swing and twist could be recorded however since the recording of data is often manual this would be an arduous task. More automated means are clearly necessitated.

Inclinometers

Single axis inclinometers are used for the measurement of angles in reference to gravity. Digital multi-axis inclinometers use micro electro-mechanical systems technology to sense tilt angles over a full 360° range in three axes would seem to be an ideal means for the recoding of motion limits. Their cost in the past may have been a prohibiting factor however they have dropped significantly in price in recent years.

Exo-skeleton

Accelerometer, goniometers or inclinometer devices are located at joints of a superstructure frame worn by the subject. The exo-skeleton can often be cumbersome and exert forces on the subject making some ranges of motion more difficult to achieve. Exo-skeleton systems are of particular use though where a live performance is required.

Magnetic and Ultrasonic

Magnetic systems utilise the relative magnetic flux of orthogonal coils to calculate position and orientation. Magnetic systems can suffer from interference. Ultrasonic systems consist of active markers emitting a high frequency pulse. The distance to recorders is calculated and triangulated through use of the known speed of sound. Ultrasonic recording is more cost effective than optical capture as the required microphones and emitters are considerably cheaper than the high resolution cameras usually employed.

The experimental apparatus of (Wang, et al., 1998) was composed of an adjustable chair, a cardan system (universal joint) and a sonic digitizer. The effect of the cardan system may have been similar to that of exoskeletons in somewhat hampering motion.

Optical Motion capture

This involves the recording of the position of markers that have been strategically placed on the subjects' body to aid in the recording of limits. These markers may be light reflective or emissive in some light spectrum through use of Light emitting diodes (LED's). Through use of one or more cameras which are sensitive to the detection of marker location in a 2-D space a 3-D position for each visible marker can be reconstructed. With emissive systems strobing the LED markers in particular sequences allows them to be uniquely distinguished and removes much of the human intervention required by passive marker system. Optical systems can suffer from marker occlusion or marker swopping where discrimination is an issue. The greater the number of cameras recording the motion the greater the confidence in the eventual reconstruction will be. Reliable reconstruction from monocular capture is area of ongoing research with multi-camera systems being more prevalent. Marker less optical capture means are a hot topic in the computer vision field, however approaches to overcome issues presented by visual ambiguities make those techniques very complex.

Completeness of data

The data set of permissible range of motion is often achieved by having the subject perform an as exhaustive repertoire of motions as time permits. The density of data may vary as covering all motion evenly may be difficult. Holes in the data set may also occur as subjects may be uncomfortable in approaching the true anatomical limits. Markers should be placed in such a manner as to enable computation of each effective rotation component. Placing markers and sensors precisely on the joint centres is not possible due to their internal nature but also any marker or sensor placed on the skin may shift as skin and tissue stretch and so introduce noise to the data.

Summary

Devices are typically placed on the subject for recording motion. The devices may be a combination of inertial analysers and acoustic or light emitters, have a magnetic property or more commonly a passive marker that is highly reflective to some spectrum of light. As already mentioned the ability for an animator to edit limits is desirable where repeated subject performances are untenable.

State-of-the-art of joint limits representations

The following research is concerned with alternative methods for the parameterisation of complex joint limits. The three main rotation parameterisations in the following research are vector twist the closely related exponential map and more recently quaternions. The main complex joint limiting techniques in research (as best I can determine) are spherical polygons, derivatives of joint sinus cones and implicit surface representation.

Spherical Polygons

A spherical polygon is a closed geometric figure formed by connecting great arcs (A great arc is the shortest path that binds two points on a sphere) between a number of vertices on the surface of a unit sphere denoting the joint limit boundary. Spherical polygons are a generalisation of spherical triangles. It is to be noted that some aspects of Euclidean geometry do not transfer to spherical geometry, such as the sum of the angles of a triangle is always greater than rather than equal to 180 degrees in spherical geometry.

Korein (Korein, 1985) describes the location of the vertices in a directed order sequence each with 3-D Cartesian coordinates. Two spherical coordinates could have perhaps have been used for the points thus reducing the storage requirement for this representation but would necessitate conversion for further processing. Also Baerlocher (Baerlocher & Boulic, 2001) suggests that the use of trigonometric functions is minimised when the spherical polygon vertices are expressed in Cartesian coordinates. The accuracy of the boundary is directly related to number and distribution of the vertices used in its construction.

To implement Korein's algorithm requires the creation of a great circle arc from the question point through any vertex of the spherical polygon and intersection tests be performed with the arcs of the spherical polygon. Korein's method for testing whether a point lies within a spherical polygon is described without the mathematical functions for its implementation. Finding such intersections in spherical space of would seem to require the use of multiple trigonometric and inverse trigonometric functions. Computation of such functions is expensive typically involving recursive calculations and as the number of boundary vertices is increased so too is the computational load. Yet the implementation in (Baerlocher & Boulic, 2001) of the point-in-spherical-polygon algorithm takes approximately 0.01 ms to 0.05 ms, for polygons with 4 to 200 edges on a SGI Octane with a 195 MHz R10000 processor, a slow machine in comparison to modern architectures. While no functions are discussed this is perhaps achieved through computation in Cartesian space reducing the number of required trigonometric functions. Through defining a plane (**Pnew)** constructed from the origin and the two points of the above great circle and a similarly constructed plane for each spherical polygon arc (**P{1-n}**), intersection lines between are found between **Pnew** and each (**P{1-n}**), and can be intersected with the sphere.

Figure 2: A spherical polygon with five directed edges.
Reprinted from (Baerlocher & Boulic, 2001)

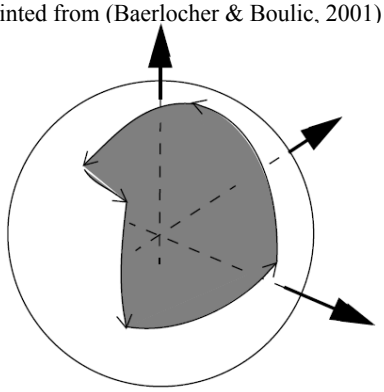

Korein's description of a spherical polygon permits a concave shape. Korein's test for point inclusion in a spherical polygon would not appear to have fixed execution as involves several searching tests to find the two points of the edge boundary closest to the test point. Korein defines only a global minimum-maximum twist rotation limit and so neglects the interdependence of swing and twist limits. No means to address complex coupling of joints is presented.

A similar method has been used by Maurel (Maurel, 2000), but with planar polygons. "As a consequence, the possible motion ranges are less general than those obtained with spherical polygons. However they may suffice for the human joints and the point-in-planar-polygon test algorithm is much simpler than its spherical counterpart."(Baerlocher & Boulic, 2001)

No means of encoding joint stress is presented in (Korein, 1985) however a system could perhaps be constructed through generation of concentric spherical polygons of varying shape with the inter boundary areas assigned a stress level. No tool or user interface is presented for the editing or manual generation of vertices. A method of using the mouse for selection and movement of vertices on the surface of a virtual sphere would not be overly difficult to implement. Equally possible would be the selecting of great arcs for subdivision and movement of the generated medial point or selecting and deletion of vertices creating a new order of directed edges.

Herda (Herda, Urtasun, & Fua, 2003) suggests that Baerlocher (Baerlocher & Boulic, 2001) addresses the parameterisation of twist by defining "local ranges of axial rotation all over the surface of the sphere". I initially took this to mean that differing ranges of axial rotation were permissible at differing locations on the sphere. While this seems a valid approach no means of encoding this data are eluded to. Their paper indicates to the contrary of my interpretation of Herda's remark with twist limits being constant over the range of swing motion even remarking that the twist limits in reality depend on the position of the arm. My approach enables encoding of twist limits at many points across a surface.

Figure 3: Baerlocher spherical polygon with global twist limit.

Reprinted from (Baerlocher & Boulic, 2001)

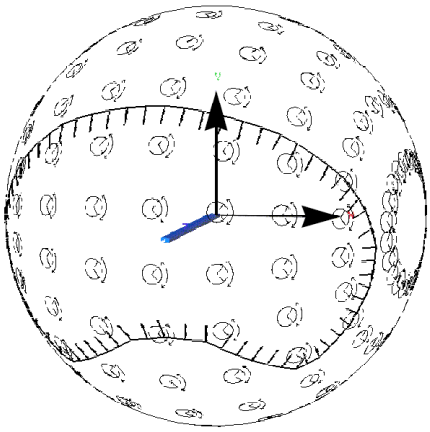

Spherical Ellipses

Proposed for use as joint limits by Grassia (Grassia, 1998). Spherical ellipses are easily parameterised needing only a centre point, an axial orientation and major and minor radii. Or can be parameterised with the constant length discussed further below and loci positions.

But are expressed more simply in (Baerlocher & Boulic, 2001) as the fulfilment of the following function: With S_x being the x axis rotation and S_y the y axis rotation of the vector being tested and $r_x$and $r_y$describing the maximum angle of rotation around the x-axis and the y-axis respectively.

Equation 4: Spherical Ellipse function

$$f(S_x, S_y) = (S_x/r_x)^2 + \left(S_x/r_y\right)^2 - 1, \qquad with\ r_x < \pi\ and\ r_y < \pi$$

As with their counter part in Euclidean geometry they have the restriction of being convex in nature. The inside outside test for a point can be achieved with the addition of two distance checks in S^2 and comparison with a known constant value. The constant being twice the length of the line from a focus point to the orthogonal minor radius (Figure 4). If the combined distance from the point to each focus point is greater than the constant then the point is not within spherical ellipse, if equal it lies on the boundary and if less than is within the bounds.

Or the swing limit can be more simply expressed as in (Grassia, 1998) as

Equation 5: Swing points within boundary

$$\left(\frac{r_x}{x}\right)^2 + \left(\frac{r_y}{y}\right)^2 \leq 1$$

Such a test is not considered computationally expensive. If consideration of a 2-D ellipse is permissible then to find a close approximation to the nearest point on the ellipse boundary for a point out of bounds (P) one might find the intersection points A & B of lines drawn from the

foci to P with the ellipse boundary. Find the intersection point C of lines from Focus 1 to B and Focus 2 to A. The line P to C is near normal and its intersection with the ellipse boundary is therefore near to the point closest to P. A similar solution could be constructed to address the spherical ellipse but the curved nature of the space introduces some complexity of calculation.

Figure 4: Determination of nearest point on 2-D ellipse boundary

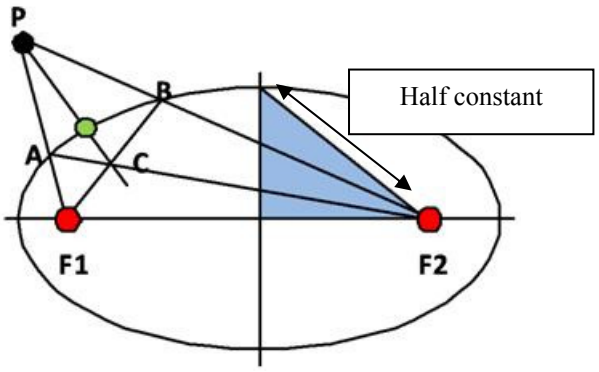

The boundary produced is of course less complex than that capable with a spherical polygon. Spherical Ellipses are restricted to a single hemisphere however while a gross simplification of the anatomical nature spherical ellipses are often considered suitable for 2-DOF joints such as the wrist where such a range is not exceeded. I have encountered no research into the interpolation of twist limits across a spherical ellipse to enable a 3-DOF representation. While the distance to boundary is easily calculable no means to create a stress map or address joint coupling in such a simple space is discussed in any research encountered.

Any tool for the generation and editing of spherical ellipses would be near trivial to implement given the simplicity of their formulation.

Figure 5: Spherical Ellipse.

Reprinted from (Baerlocher & Boulic, 2001)

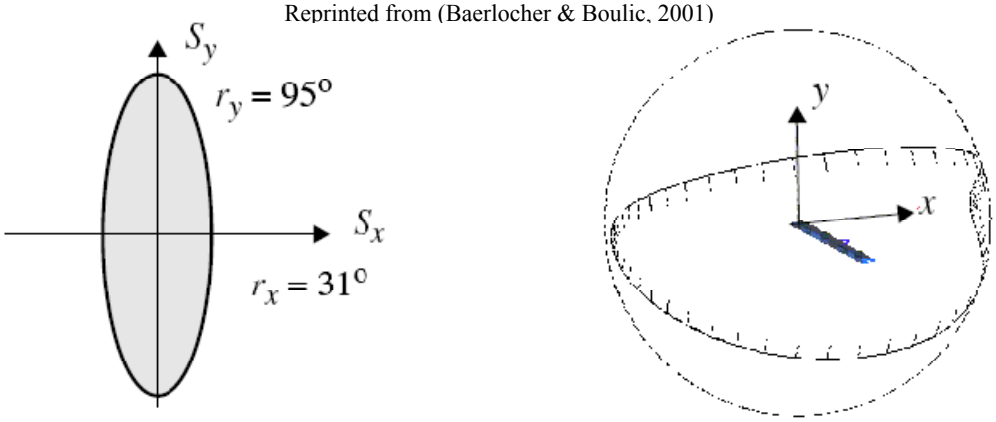

Triangular Bézier Spline Surface

Proposed by Tolani (Tolani, Badler, & Gallier, 2000) this method constructs a model using experimental (motion captured) data for the position and orientation range of the upper arm through measurement of marker distance from other joint positions. The permissible elbow workspace is then described by a triangular Bézier patch as it may be subdivided efficiently pruning the search space for the solving of inverse kinematic problems. They record 100 to 200 points of imperial data and suggest a surface derived from 35 control points produces a reasonable surface model for this task.

The search space is narrowed through coarse intersection tests made efficient though an Octree data structure. Fine level intersection tests with the surface are achieved at the triangle polygon level with sphere triangle testing.

Figure 6: Distance of the elbow from the humerus and the corresponding Bézier surface fit.
Reprinted from (Tolani, Badler, & Gallier, 2000).

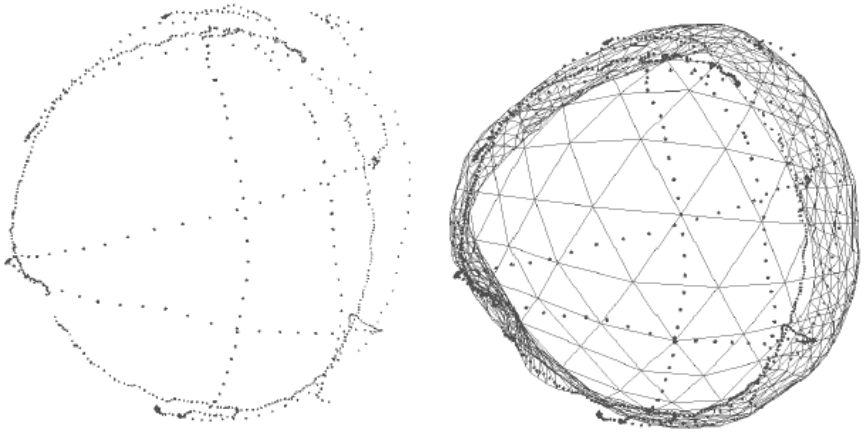

An interface permitting the movement of control points for this method is possible and would produce a different surface. However to avoid a trial an error approach the user would have to be knowledgeable of Bézier constraints and as can be seen from (Figure 6) the complexity of surface geometry makes it a decidedly unattractive proposition as implied in (Tolani, Badler, & Gallier, 2000) “coordinates on a Bézier patch are unintuitive and should be concealed from the user”. To edit the subdivided mesh vertices would also be achievable in any 3-D package supporting Bézier surfaces however doing so may require recalculation of control points (perhaps through a least squares approach) or the abandonment of the Bezier formulation to store the mesh as vertices. To store the three Cartesian coordinates for a finely tessellated surface mesh is achievable utilising triangle winding order formats common for 3-D model storage in video games. But the results of editing of the mesh would be difficult to intuit.

The Tolani surface model defines only the angular motion (swing). The restriction of twist is modelled as a separate single function of elbow elevation (see Figure 7). As with implicit surface methods the fit of the surface to the data is imperfect and susceptible to error due to undersampled data regions.

Figure 7: Twist defined as a function of angular motion. Linear Least Squares fit.
Reprinted from (Tolani, Badler, & Gallier, 2000).

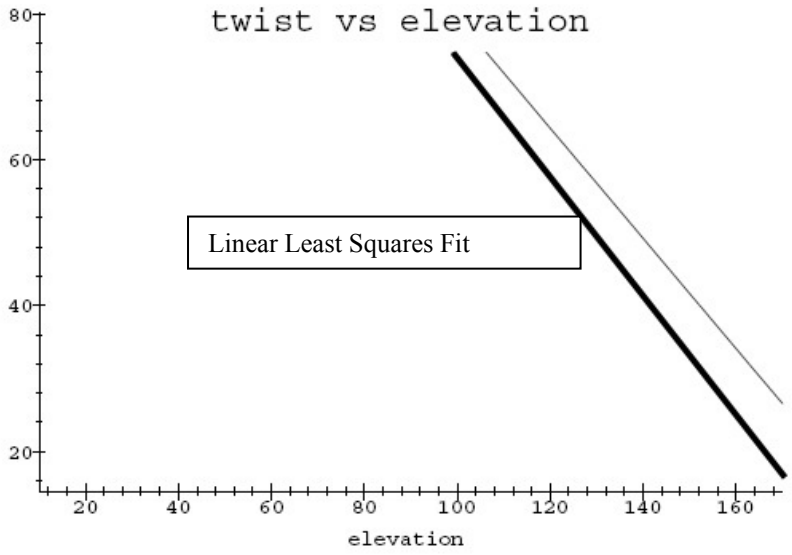

Joint Sinus Cone

Joint sinus cones and spherical polygons are closely related. Engin and Tümer's (Engin & Tümer, 1989) investigation of joint boundaries presents sinus cone parameterisation. In their approach joint boundaries are constructed of conic shapes with distorted ellipsoid planar bases in the local space of the joint. The apex of the conic shape being located at the functional centre of the joint. The joint sinus cone basis curve is described as a two-dimensional closed polygon enclosing valid vector orientations for the bone. At a distance along the cone axis (often unit or length of bone) a 2-D planar polygon defines a boundary setting the upper limit in any given vector direction. The 3-D problem of testing if a bone vector lies within a curve on a spherical surface is so reduced to a two-dimensional point-in-polygon test, a well researched problem in geometry.

One way to perform a 2-D point-in-polygon test is to "compute the sum of the angles made between the test point and each pair of points making up the polygon. If this sum is 2π then the point is an interior point, if 0 then the point is an exterior point" (Bourke, 1987). This and other methods such as ray intersection count tests are commonly applied in graphics applications.

In (Engin & Tümer, 1989) the shape of the sinus cone was derived from in vivo observations of subjects. Engin and Tümer generated multiple cones for the shoulder joint complex each expressing the range of motion of the component joints (Figure 8). Maurel (Maurel, 2000) utilises an ellipsoid constraint combined with joint sinus cones. However for ease of calculation it is often desirable that the shoulder complex be simplified to single joint which differs from the anatomic reality. For this reason a composite joint sinus cone can be formulated (Figure 9).

Figure 8: Shoulder joints sinus cones.

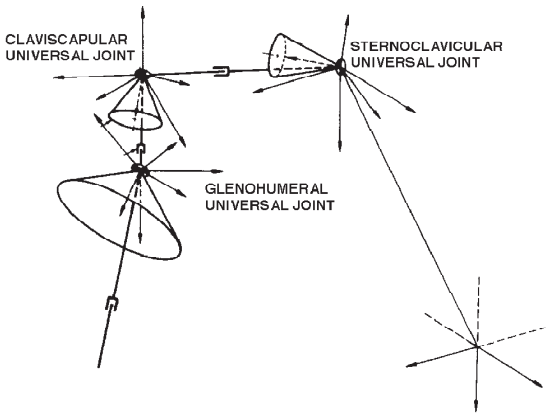

Reprinted from (Engin & Tümer, 1989)

Figure 9: Composite of the above three cones and its cross section

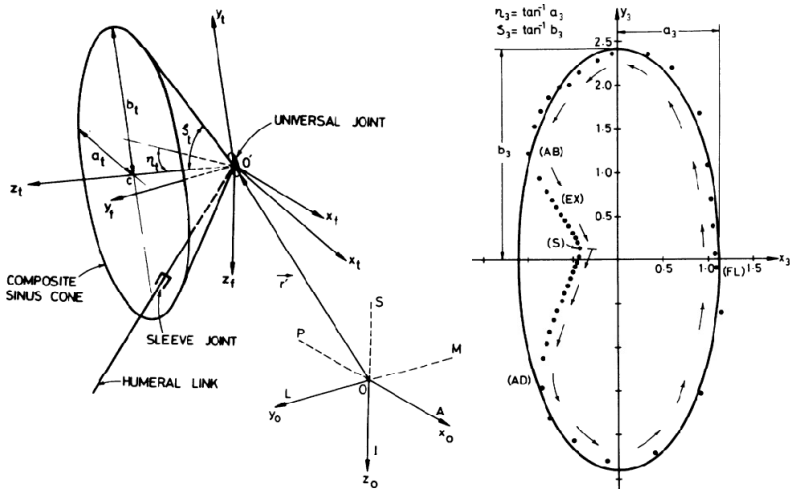

Reprinted from (Engin & Tümer, 1989)

Having performed the inside outside test the next challenge lies in respecting the limits of the conic boundary requiring the bone vector be altered when found to be beyond the limit. Maurel suggests this be achieved through "Line segment-intersection test applied to the radial limb with each segment of the cone basis" Figure 10 (Maurel, 2000). For a complex boundary consisting of many vertices such an approach would result in many such tests. The method I will present pre-computes the corrective boundary position for a given swing vector with the aim of reducing runtime computation.

Figure 10: Correction of point outside boundary.

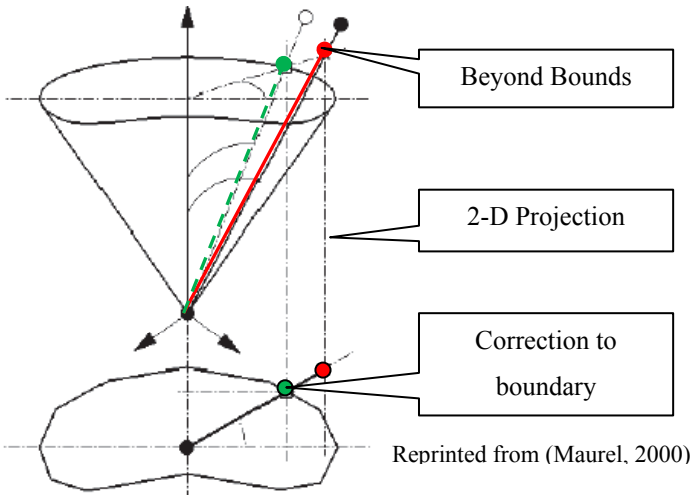

Reprinted from (Maurel, 2000)

Maurel (Maurel, 2000) addresses the development of an editor allowing the interactive design of joint sinus cones (Figure 11). Their tool permits the selection of joints and the adjustment of joint ranges of motion.

Features of Maurel Tool

- The 2-D interactive design of the cone basis polygon
- The setting of the cone orientation with respect to the skeleton
- Motion control of the limb segment for interactive testing of the cone

Figure 11: User interface to Maurel tool.

Reprinted from (Maurel, 2000)

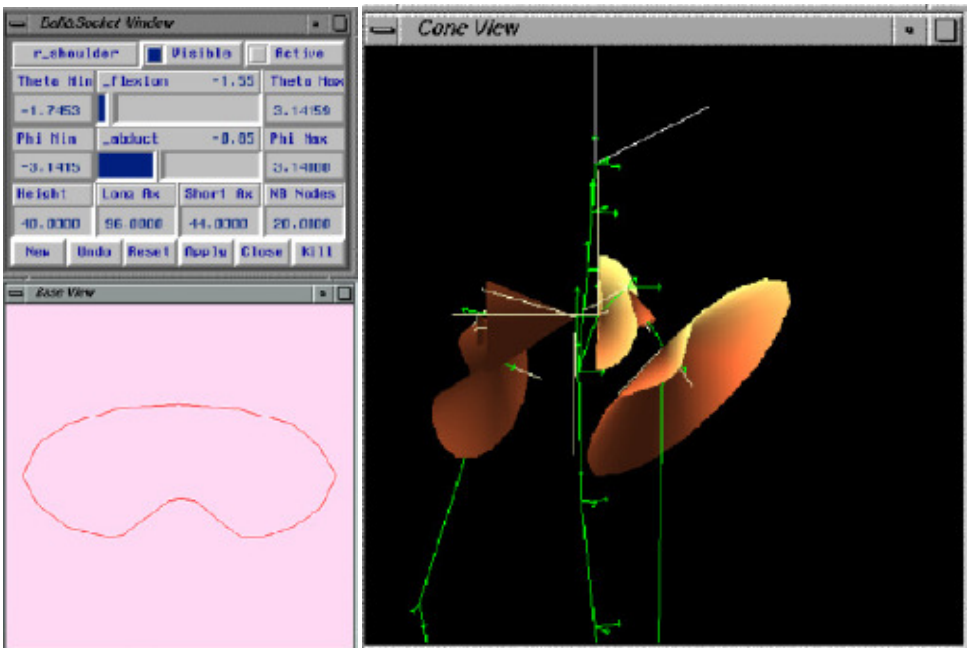

The need for the user to interactively orientate the 3-D cone with respect to the skeleton presents an added complication as does the initial setting of the long and short axes of the elliptic basis.

Shown in pink (Figure 11) a 2-D panel displays the polygonal basis of the current cone. “In this area, the user can interactively design the shape of the polygon by picking and dragging the existing vertex. Vertex addition can be achieved individually using the mouse or globally by setting the vertex number in the control panel. On the contrary, vertex removal is only allowed individually with the mouse” (Maurel, 2000). While quite intuitive to alter the elliptic basis through point addition and dragging to create a complex polygon of many vertices would be very repetitive. However the benefits of a 2-D editing system are recognised. I will present a pixel based texture editing system enabling the painting of the boundary.

The interactive direct posing of the limb to test joint boundaries is considered a sound approach and will be replicated in my system. With each cone limited to one hemisphere or less the use

of multiple cones increases the complication of the system for animator control. Maurel suggests the use of multiple cones to address unrealistic deformations of the overlaying layers. I would consider that advances in this area such as dual quaternion skinning may in part address such issues. I consider Maurel's embedment of the tool in a non-commercially available system as a major impediment to its adoption. The most glaring omission of a joint sinus cone is that it presents no limit on the permissible twist. The method I will present addresses this short coming.

Given a set of control vertex positions (Shao & Ng-Thow-Hing, 2003) utilise subdivision rules to refine and smooth the boundary curve of their sinus cone (Figure 12). In an attempt to address the issue of lack of a limit on twist Shao et al introduces a pair of angle bounds associated with each control point on the curve which are interpolated during the curve subdivision and also radialy to a point V_{rest} lying on a vector from the cone apex in the direction of the bone's longitudinal axis at its rest configuration. Interpolation of twist for a point within the bounds is performed at run-time. I will present a pre-calculation of twist across the domain which can be more complex than achievable with the above system and removes the run time calculation overhead.

Figure 12: Subdivision of boundary. Right: Runtime interpolated twist limit range

Reprinted from (Shao & Ng-Thow-Hing, 2003)

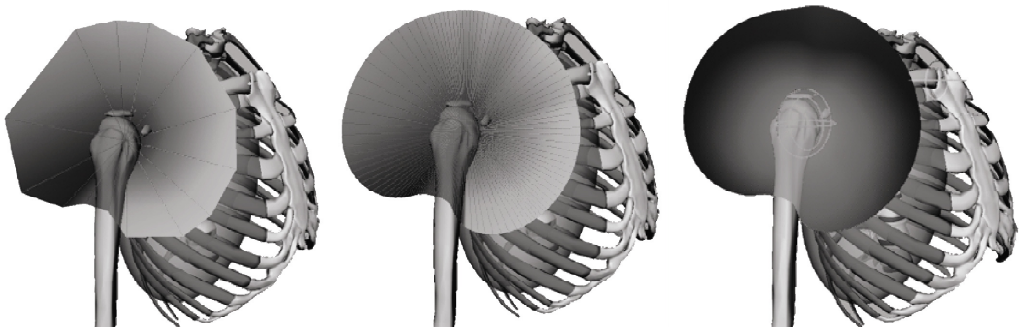

"On the right, the cone is shaded based on the twist limits on each point. Darker shades indicate a more restricted limit range"

"Custom plug-ins were developed for the Maya 3-D modelling software to allow interactive placement of the bones and adjustment of joint parameters" (Shao & Ng-Thow-Hing, 2003). I have been unable to locate this plug-in within the public domain.

Reach Cones

Wilhelms's (Wilhelms, 2001) presents a system similar to both Joint Sinus Cones and Spherical Polygons called "Reach Cones". Reach cones are not limited to one hemisphere and also address twist limits in a similar fashion to (Shao & Ng-Thow-Hing, 2003). Rather than a 2-D point in polygon test as previously discussed Wilhelms's inclusion and intersection tests are three-dimensional.

Reach cones require an additional point similar to (Shao & Ng-Thow-Hing, 2003)'s $V_{rest.}$ called a "visible" point for which any great-circle arc (or line segment) joining a boundary point with the visible point lies entirely inside the reach cone. This visible point is again used in the interpolation of twist ranges to the outer bounds but utilises weighted barycentric coordinates.

Figure 13: A reach-cone polygon with 5 boundary points and a visible point is shown.

Reprinted from (Wilhelms, 2001)

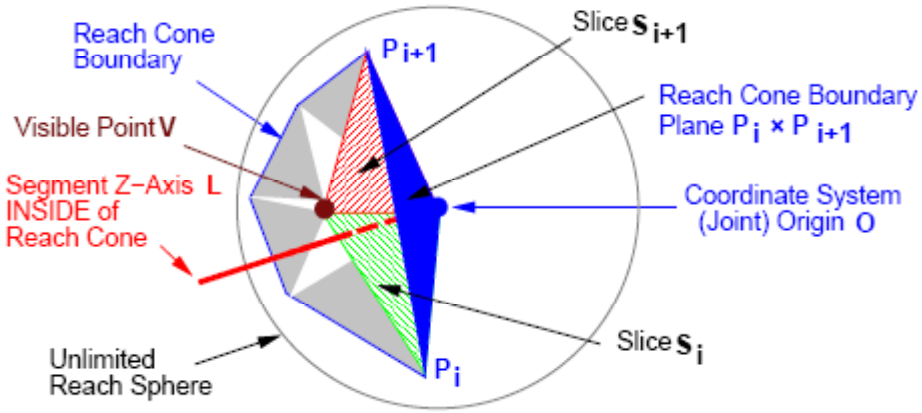

Detecting if a point is contained within the reach cone boundary requires finding the sequential pair of planes (shown in red and green above, called slices) whose normals when dotted with the point give a possitive value and then perform the same test with the plain connecting the boundary points of those plains and the origin (shown in blue) and the point. The efficieny improvement of this technique lies in the fact that the normals of each slice can be pre-computed using the cross product. Their solution for finding a boundary point for points beyond the limit is achieved by testing dot products with sequential boundary planes and then finding the slices satisfying a positive normal. Once the boundary plane has been found a straight forward intersection test is performed between the boundary plane and the line formed from the last valid position and current invalid position.

A tool with a GUI (Graphical User Interface) was created in the course of their research. No screen shots of user interaction are provided and tool does not appear in public domain. A boundary point is created interactively within their GUI by rotating the unit bone vector to the boundary point and then making a selection with the mouse. "The user can add and delete points at any location on the sphere, and designate the order of the points to define the reach-cone polygon." As with (Shao & Ng-Thow-Hing, 2003) they present a means to interpolate boundary points smoothing the curve. The same editing problems exist.

Quaternion Implicit Surface

As already mentioned assuming only rotational joints any joint limit can be expressed as a subset of a unit quaternion sphere. Herda's method involves the recording of unit quaternions from motion capture encapsulating both swing and twist. By retaining only the vector component of the quaternions they can be plotted as points within Euclidean space. The resulting point cloud generates a volume contained within a unit sphere. This volume is converted to an implicit surface through a meta-ball generating algorithm.

Once the implicit surface is generated any new quaternion vector is tested against it by finding the nearest meta-ball to its position and checking if the point lies within its spherical radius. If not then further processing is performed to account for the influence of neighbouring meta-balls on the meta-ball surface. If contained by the surface the quaternion is valid. A search along the gradient field of the surface determines the closest valid orientation when beyond the surface. This is made possible by the well-defined distance measure between orientations defined by quaternions.

Figure 14: Implicit surface generated from point volume

Reprinted from (Herda, Urtasun, & Fua, 2003)

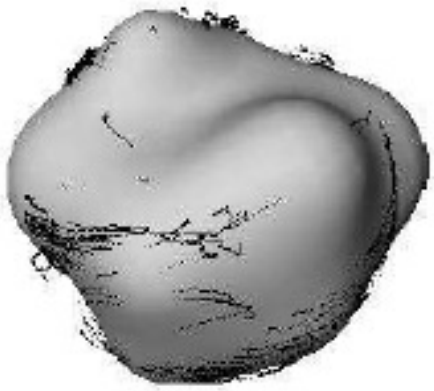

The way in which the implicit surface is generated can result in some artefacts. Herda's implicit surface parameterisation limits the number of primitives contributing to the iso-surface for ease of limit evaluation. Where the volume is complex Herda's algorithm has the tendency to cover holes in the data making ranges which may be truly unreachable permissible. An interface for making adjustments directly to the implicit surface is not presented. I would suggest that use of 3-D sculpting tools would be possible if converted to a polygonal mesh and then an implicit fit performed for this new volume could be calculated. However an intimate knowledge of the quaternion space would be required to perform such editing. Herda suggests the cloud of points can be added to from repeated motion capture sessions or the below mentioned tool and so the surface can be re-evaluated.

To address hierarchical joint limits such as that between the shoulder and elbow joint Herda presents in (Herda, Urtasun, & Fua, 2005) the association of an implicit surface to each voxel (A voxel defining a local cluster of similar joint positions) of the shoulder implicit surface. The

storage of the many required child implicit surfaces makes this solution somewhat unwieldy and again given the shapes of the surfaces it would be difficult for a user to intuit the limits visually.

Figure 15: Voxelised shoulder surface and associated child surfaces

Reprinted from (Herda, Urtasun, & Fua, 2005)

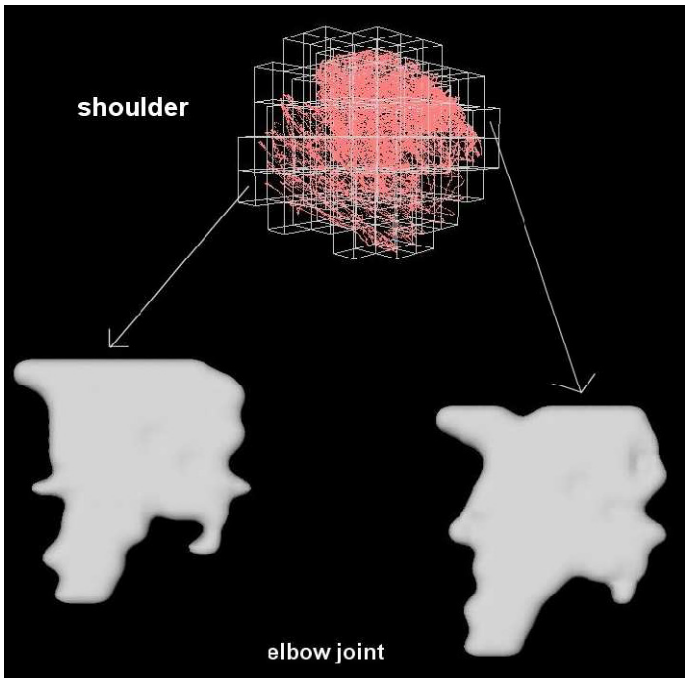

While Herda uses a tool known as "WinSceneGraph" this program does not seem to appear in the public domain. I am basing any conclusion about this tool based solely on the user manual of this application found at http://vrlab.epfl.ch/~lorna/docs/WinSceneGraph.pdf. Its main function seems to be the processing and conversion of point clouds as generated from motion capture or loaded from a file. Point clouds may be expressed in Quaternion or Cartesian formulations. The tool seems to permit the addition of points to a data cloud by entry of rotation values. Whether these values can be entered through a visual posing of an armature is unclear. The tool generates the required values for an implicit surface. Whether this surface can be displayed and intuitively edited within the tool interface is also unclear. See appendix (pg.56, Figure 44) for list of conversion menu functions.

Joint sinus accumulation buffer

The approach most similar to my own is presented by (Jing & Prakash, 2000) and utilises a Theta Phi decomposition of all valid vectors of a joint sinus to an accumulation buffer reducing point within bounds test to a simple lookup with binary result. They do not seem to consider the graphical editing of the accumulation buffer as a texture. Their approach also makes no attempt to encode permissible twist.

Figure 16: Phi Theta decomposition of a point within joint sinus.
Reprinted from (Jing & Prakash, 2000)

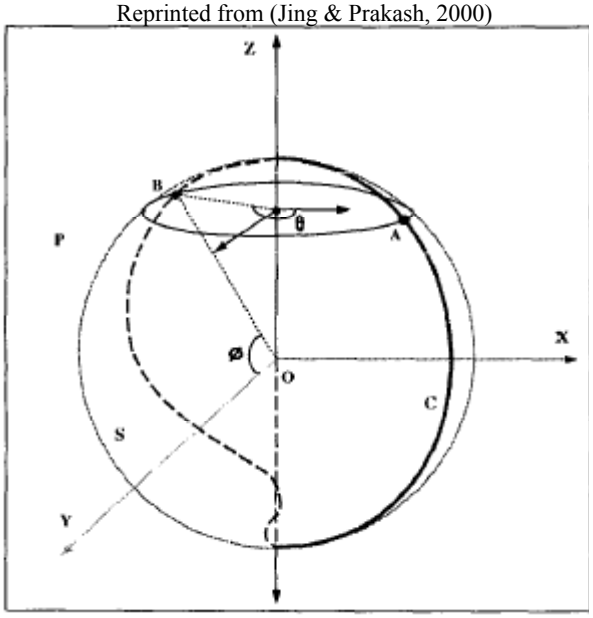

Quaternion based accumulation buffer

(Liu & Prakash, 2003) use a standard unit quaternion parameterisation in their work. However while stating that rotation limits form a region in 3-sphere they only discuss the workings of a swing limit and do not address twist.

Their formulation of a look-up table differs from my own. Their method can be summarised as follows: To rotate from a reference vector (**a)** to another (**b)** an axis of rotation (**u**) is utilised. **u** is unit length and generated from cross product of **a** and **b**. The range of motion is restricted by placing a limit on the permissible rotation about any given **u.**

If **a** is chosen to be the z-axis then **u** which lies on the orthogonal plane XY can be parameterised with and angle Φ measured counter clockwise from the positive x-axis. Φ can be quantised 0 to 360 degrees. The permissible rotation about **u** is encoded as a value between zero to one, the result of the cosine of half the angle, and so the below look-up can be generated.

Figure 17: Limit look-up table. Area is yellow is the valid range.
Reprinted from (Liu & Prakash, 2003)

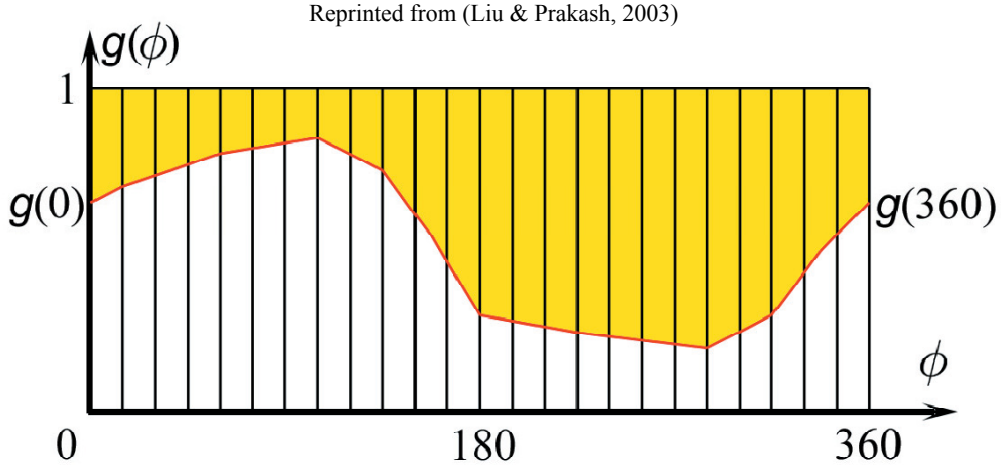

I consider this formulation very novel and may adopt it in future work however twist is not discussed in their work (though clearly could be addressed in the same manner I will propose). Nor are the other benefits made possible through a discretisation of limit boundaries that I will be presenting.

Summary

While lookup tables have been found in existing research their description as a texture suitable for GPU execution has not. With the exception of Herda's work no approach solves the dependency of twist and swing in a satisfactory manner. While a sinus cones are conceptually intuitive Herda's implicit surface representation is by far the most complete joint limiting system currently in existence. The use of a quaternion rotation formulation is desirable. Tools in this space are sparse and not publically available.

Artefact Design and Implementation

Methodology

It was intended that a prototype extension to the Blender 3-D package be created to act as a test bed for a texture based joint limit solution. The standard Blender install currently only permits Euler angle rotation limits. To show that my system is an improvement over this a comparison of permitted range of motion is to be performed.

Detailed timing information of existing techniques is not provided in many of the papers upon which my literate review was based and so hampers a comparison. As the proposed system is intended for GPU execution a shader program written in the High Level Shading Language standard (HLSL) is used for evaluation. Though use of the FX Composer 2 shader analysis tool from NVIDIA, a count of the functions required and their timing information can be obtained. From this it should be determinable if the solution is computationally prohibitive or not for its application in a video game execution environment.

Prototype Programming

A rapid development approach was adopted with continuous revisions to the system being created throughout the research timeline. Programming was performed in the C programming language. Python scripting was often used to test ideas but was later converted to equivalent C code. Microsoft's Visual C++ Express Edition was the development environment used.

Angle Parameterisation

"The swing-and-twist parameterisation is useful for dealing with ball-and-socket joints, and is a good basis for the definition of simple yet meaningful joint limits" (Baerlocher & Boulic, 2001). For this reason it is the swing-and-twist parameterisation which is the basis of the solution though where possible quaternions are used where interpolation is required.

Virtual Body Modelling

A detailed polygon mesh of a human male was modified to provide a suitable character for manipulation. The entire mesh consists of nearly 8000 vertices creating over 14000 faces. Within this mesh the character forearm, upper arm and torso are separate mesh loops. This separation was performed to enable easy selection of vertices for bone influence assignment and also to remove consideration of possible skinning issues which while addressable in Blender through dual quaternion skinning are not the focus of this research.

Figure 18: Character Mesh

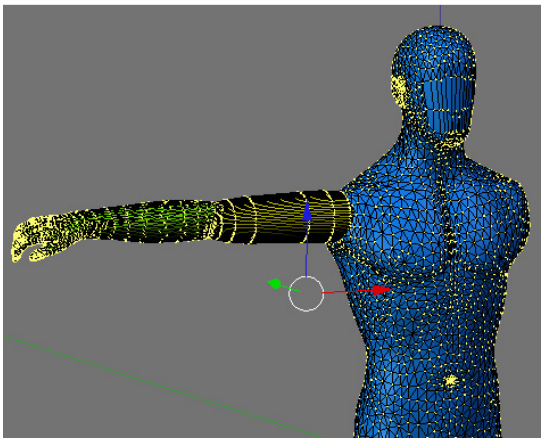

Skeleton Modelling

A simple armature was constructed within the mesh (Figure 19) of a similar design to that seen in video game characters (pg.58, Figure 51). The creation of the armature rig with arms outstretched from the body is a commonly used in video game character assets and is referred to as the initial “T pose”.

Figure 19: Character armature

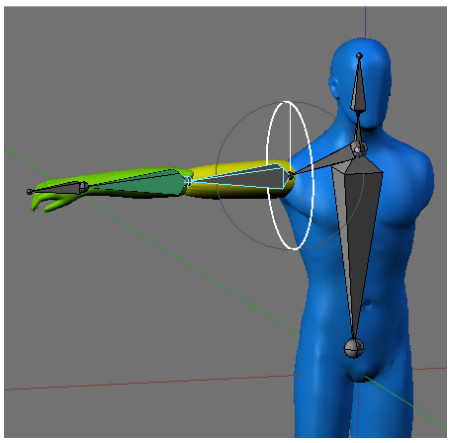

Model Posing

As shown in (Figure 20) once vertex-bone associations have been created the existing features of Blender permit the posing of the armature bones to affect the character mesh posture. However the existing mechanism for posing the armature bones through direct entry of rotation

angles or use of the rotation manipulator is considered unwieldy particularly as the trackball movement (pg. 56, Figure 45) seen in other packages appears absent from Blender. To address this problem a UI element was developed (Figure 21) which was derived from a Blender UI element used for setting lighting directions and was named the “pose helper”. Through interaction with the 2-D sphere via the mouse the direction vector (swing) of the selected bone could be set. For the upper-arm bone with the red circle of the pose helper obscuring the black circle the pose would be set to the default T position as in (Figure 19). When the direction vector is within the opposite hemisphere to the T pose this is indicated to the user by changing the colour of the vector line and circle to blue (See right Figure 21).

Figure 20: Armature posing

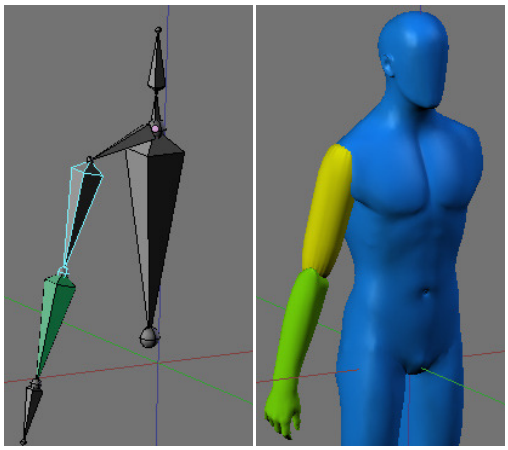

Figure 21: Pose Helper

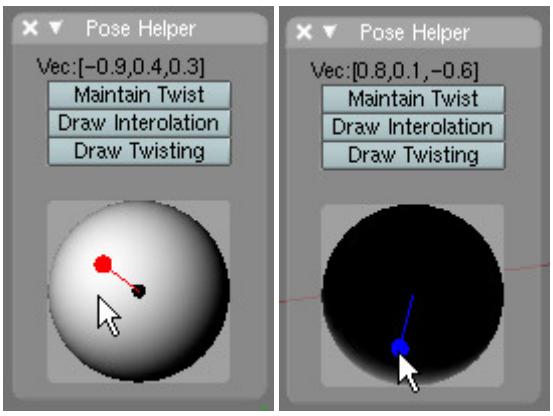

The vector returned from the pose helper UI was converted to an armature bone pose as follows. First the rotation about a fixed axis was calculated (Positive Y was chosen). This is done by calculating the arc cosine of the dot product of the two vectors. Then the orthogonal vector to each vector was calculated by using the cross product. This allows formulation of pose as a Vector and Rotation which is easily converted to quaternion form (Appendix pg.59). In Blender each bone has a quaternion parameter. Having set the quaternion all that is required is to call a recalculation of pose matrices and call a draw function to display the result on screen.

Quaternion Pose Code:

```
Rotation=acos(Inpf(Unit_Yaxis_Vector, PoseHelperVector)); //Arc Cosine of Dot Product
Crossf(newVector, PoseHelperVector, Unit_Yaxis_Vector); //Cross Product
VecRotToQuat(newVector, Rotation, PoseQuaternion); //Conversion to Quaternion
```

Sinus Texture Generation

Through use of the pose helper the user sets a given swing vector for the selected bone. Successive swing vectors are interpolated and as seen in the poser helper UI the user may choose to see the interpolated motion between the vectors by clicking the "Draw Interpolation" button. The number of interpolation steps between the start and end vector was determined by the magnitude of the angle between them, again calculable from the arc cosine of the dot product of the two vectors.

Interpolation was necessary to ensure good vector coverage between start and end vectors as to use the mouse control to cover the range would be difficult given the low speed of its response polling. For ease of coding a simple linear interpolation was performed with each generated vector being re-normalised. While sufficient given that the interpolation step was small and a discretisation of vectors would follow in the texture map generation, it would be desirable to implement spherical interpolation for clarity of solution. It was desired that as the pose helper sphere was manipulated that the bone swing vector update in real-time. This was not achievable due to the current structure of Blenders UI code which is not designed to permit updates to the 3-D view screen while a UI element is in use. I have been informed this impediment will be resolved in the next major release of Blender.

For each normalised interpolated vector its angle θ to the negative Y-axis was calculated using the arctan2 function (arctangent in $-\pi$ to π range) with the Y and Z vector components as parameters (Figure 22). Two such angles (the other measured against the X axis) could have been used to describe the vector. However I chose to represented the vector as an angle and a radius measured against the Y&Z axes. Note this radius does not equal the true radius from the 3-D point to the origin but is a 2-D projection. This was performed by Pythagoras theorem taking the square root of the sum of $Ycomponent^2$ and $Zcomponent^2$. The value of θ was mapped to a range of zero to the pixel width of a set image file. The radius value was mapped from zero to half the height of this same image.

Figure 22: Theta and Radius calculation. Blender Coordinate System

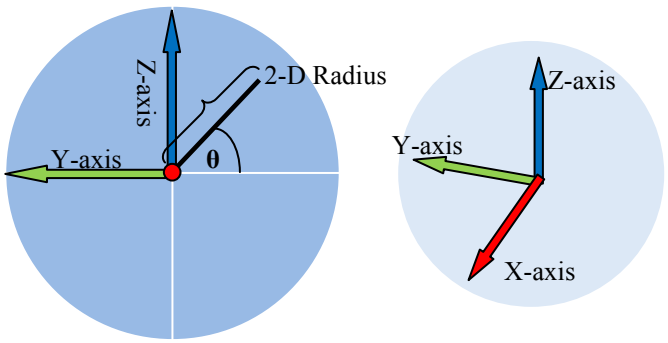

During testing an image of 256 x 512 pixels was used. Radii of vectors with a positive X component take up the bottom half of the image with the radius lengths from zero to one mapped to pixel height 0 to 255 measured from the bottom. While the radii of vectors with a negative X component occupy the top half with lengths of one mapped to the mid height of the image and 0 at the image top. The image space can be considered to be divided into two hemispheres.

Point within boundary test

To determine if a given swing vector is within the sinus boundary its x and y pixel coordinates are calculated as above. If the pixel value of the red channel is 0 at those coordinates then the point is invalid otherwise the vector is within the sinus cone and considered valid. Such a pixel look up is computationally inexpensive for modern GPUs and will be discussed later.

Figure 23: Sinus Cone Texture

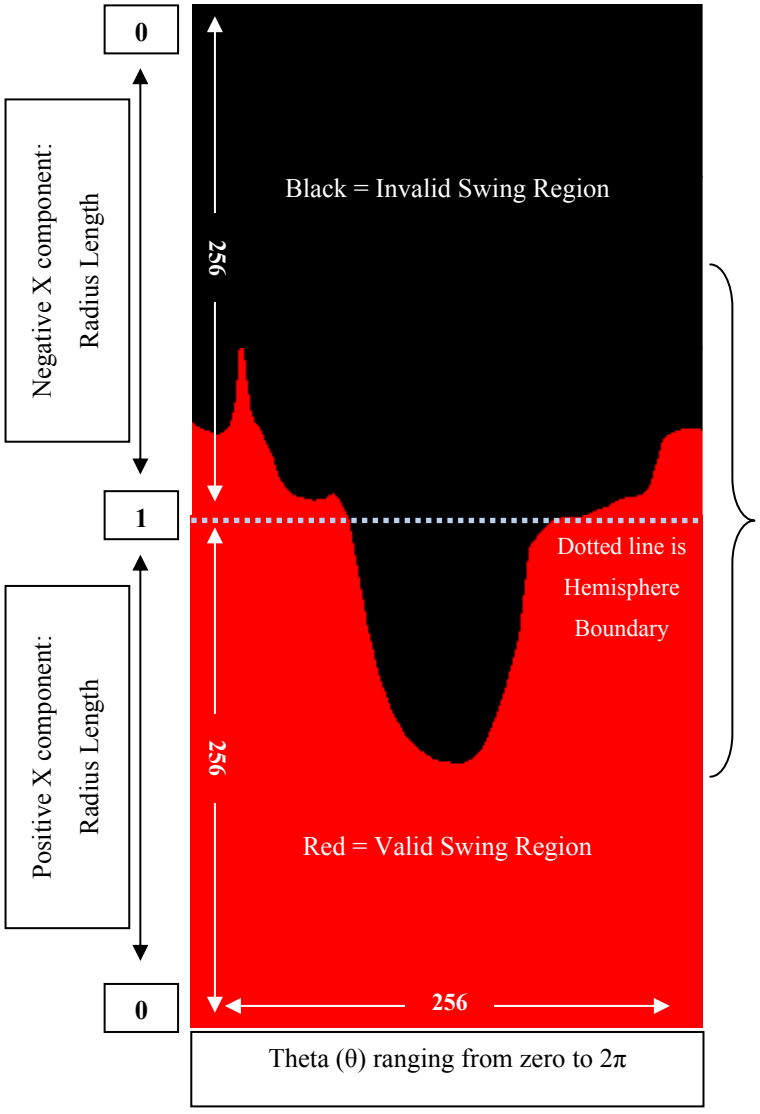

Sampling issue with the texture

While the 255 vertex points for the sinus cone is significantly more than that seen tested in other research the proposed system necessitates that the points be evenly distributed. Regions of high gradient change may not be sampled sufficiently. Rather than a somewhat smooth pixel curve a significant step effect of pixels is seen in these areas. This is addressed somewhat through higher resolution textures but I have not presented a means to increase the number of vertices in an area. The concentration of vertices is adjustable in existing research. To consider these steps as control points for a curve could be explored however the advantages of a simple pixel boundary test are then removed.

Figure 24: Zoom in on pixel step effect

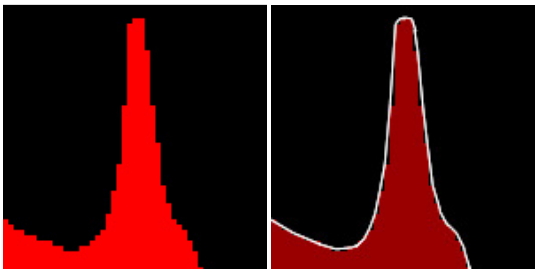

Sinus Cone Visualisation

While a texture rather than a 3-D sinus cone is used in limit calculation I consider sinus cones a useful visual representation of swing limits. For this reason I decided that displaying the sinus cone would be of benefit particularly for users already familiar with such a representation. To do so a polygon cone with non closed circular base having a number of vertices equal to width of the sinus texture was generated, with one vertex being the apex. Then through finding the pixel height value of the red/back pixel boundary for each image column and converting these x and y pixel coordinates back to vector form a 2-D array of vectors was generated. The vertex array of the circular base cone was then set to this 2-D array producing the sinus cone as shown in (Figure 25).

Conversion from 2-D Pixel coordinates back to a Vector:

```
float Vector[3];
float recoveredRadius;
float theta=(x*(2.0f*(float)M_PI))/((float)width);

if (y>(height/2))
{
      y=(height-y);
      recoveredRadius=((float)y)/((float)(height/2));
      Vector[2]=-(sqrt(1.0f-
(recoveredRadius*recoveredRadius)));
}
else
{
      recoveredRadius=((float)y)/((float)(height/2));
      Vector[2]=sqrt(1.0f-(recoveredRadius*recoveredRadius));
}
Vector[0]=(cos(theta))*recoveredRadius;
Vector[1]=(sin(theta))*recoveredRadius;
```

Figure 25: Circular Base Cone and resulting Sinus Cone

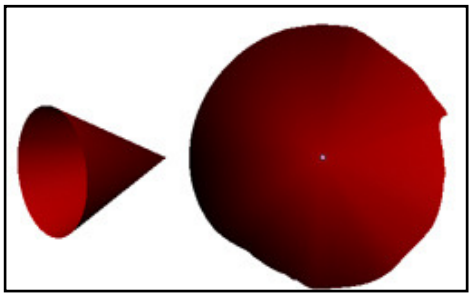

Sinus Boundary Animation

A button was provided for the user to see the effect of the sinus boundary causing the selected joint to move through the 255 vector positions of the boundary. Interpolation while easily implementable was not considered necessary for this visualisation. It is noted however that as expected from (Figure 24) the animation is not of a constant acceleration. Discontinuities occur as no interpolation based on a distance measure between vertices is being performed here.

Figure 26: UI Panel and Boundary Animation

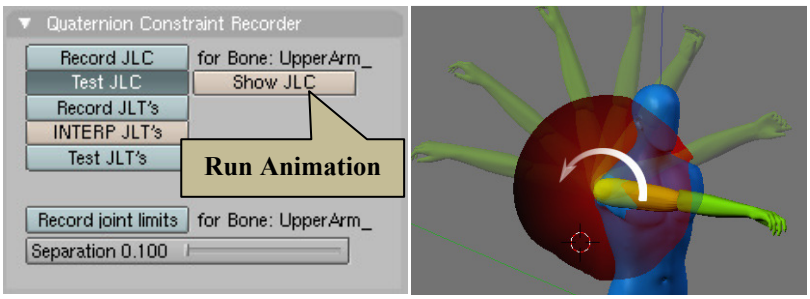

Editing of Sinus Texture

Blender already has basic pixel painting tools. To aid in the editing of the sinus texture two brushes were setup for convenience to paint black and red pixels onto the texture. A contiguous area of black was not enforced and so holes could be created which would be analogous to non-overlapping spherical polygons (See Appendix pg.59, Figure 52). Though as noted in (Baerlocher & Boulic, 2001) such holes are perhaps unnecessary for human joints. For ease of use any future development should perhaps ensure only two distinct regions are created. The creation of overhangs is also possible (Right Figure 27). The Sinus cone of (Figure 25) can be updated to match texture boundary by clicking the "Test JLC" button of (Figure 26).

Figure 27: Pixel editing tool

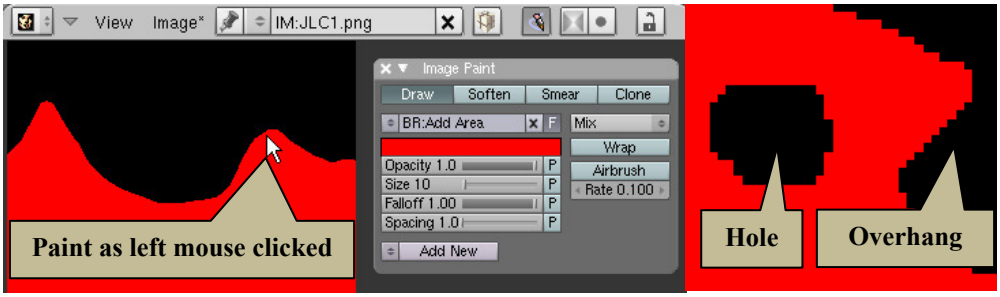

Consideration of Limit avoidance and Stress Measurement

The texture format for the sinus limit provides a convenient mechanism to also encode stress or the encroachment upon the boundary curve. As will be presented with twist, values could be set at key joint articulations and interpolated. These key values could set through presenting a slider bar UI and may be based on feedback of discomfort from a live subject. However given the intuitive mapping of the texture a painting of stress with pixel tools was approached. White was used as the colour to indicate a high stress level with black being considered no stress (Figure 28). A graduation was performed respecting the boundary curve. This gradient map could be integrated into an Inverse Kinematics (IK) system performing least resistance path finding. Also shown in blue (Figure 28) the degree to which the boundary could be exceeded before a change of simulation would be required can also be mapped. This was intended to be used to show when a joint would be broken had a force from a physics system placed the joint in such an orientation.

While Blender provides a way to set soft edge brushes the stress map generation process is more suited to dedicated graphics editing package such as Adobe Photoshop were gradient generation tools may be of benefit.

Figure 28: Stress Map

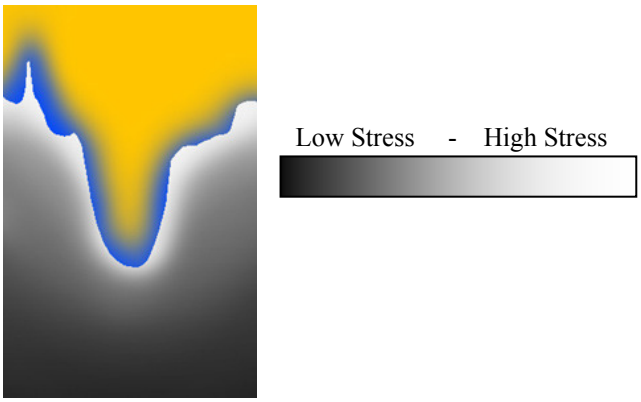

Correction of point beyond boundary

Considered in isolation

If presented with a vector beyond the sinus boundary and no consideration is given to any previous vector then at that vectors pixel position a reference to its nearest valid boundary point can be pre-computed. Given that a pixel in the joint limit texture that has a zero red channel value is considered out of the sinus bounds then the green, blue and alpha channel of that pixel are unutilised. If the Green channel 0-255 is used to directly index the X position of the nearest valid boundary pixel then the addition of the blue and alpha channel values can index the Y position (0-511) of the valid boundary point (Figure 29 right)

Noting that offline computation can be as complex as desired to find the nearest valid boundary point a temporary array of all boundary pixels was constructed. The angle between the corresponding vector of each entry of the array and the vector of the point beyond bounds was

calculated (Arccosine of Dot Product). The angle in radians is equal to the length of the arc joining the two vectors (Figure 29 left). A reference to the pixel yielding the smallest length arc was stored. A 2-D pixel distance measure was also programmed for testing purposes but was not deemed suitable given the curvature of the true space (Figure 30)

Having performed a pre-computation for each pixel of the joint limit texture with a zero red channel value the correction of a vector beyond the sinus boundary simply involves the conversion of the vector to a pixel lookup and a conversion back to a vector of the value stored by that pixel. This is considered highly efficient and easily achieved for an image of 256x512 pixels or less. At larger texture dimensions (unless split into multiple textures) due to the limitation of 8-bits per pixel channel it may only be possible for a point in the region of the nearest point to be referenced and so require a subsequent local search.

Figure 29: Arc distance measure Pre-computation

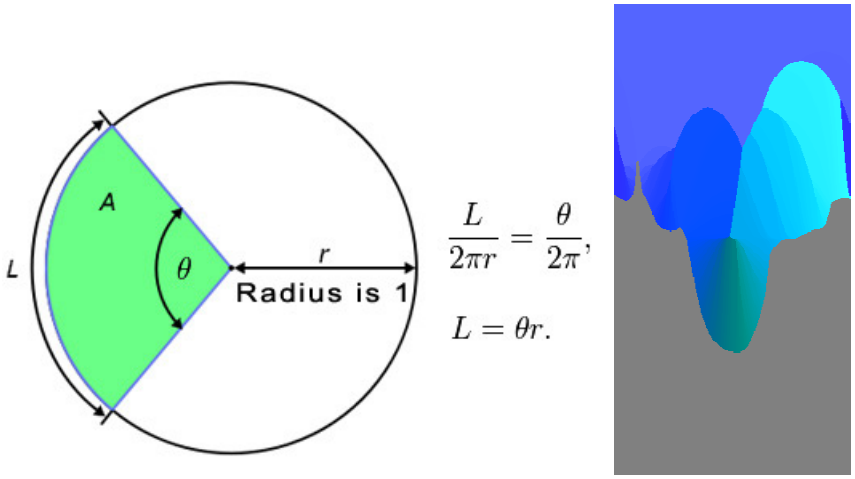

Figure 30: 2-D distance measure Pre-computation

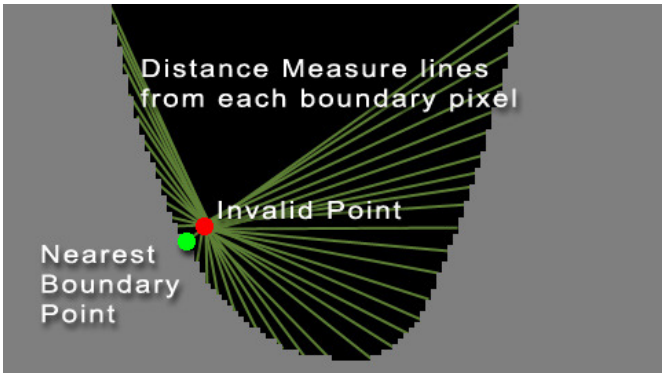

Should the exact corrective boundary pixel not be index able then at run time the localised search would be performed as follows. The number of pixels to cast the invalid point vertically to the boundary (just downward if pixel overhangs are not permitted) is recorded as is the number on either side of the point in the horizontal. The projected boundary point having the lowest pixel distance to the invalid point becomes the start point of a boundary search. The direction along the boundary is followed while the distance to invalid point is reducing and so a corrective point is converged upon (Figure 31 right).

Figure 31: Binary Search Boundary Correction

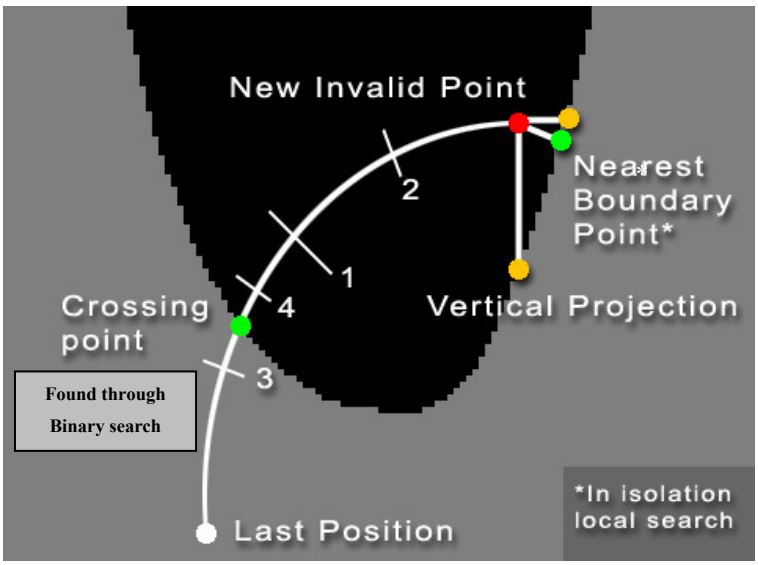

Considered with known last valid position

If an animation has a previous valid swing position and new invalid swing position then it is assumed any interpolation between these points would occur along a great arc between them. This great arc would intersect the boundary curve and the intersection point should be the corrective boundary position. A binary search along this curve is proposed to converge on the crossing point at runtime which is to be the corrective boundary position but was not implemented in the artefact. The midpoints would be generated from interpolating linearly between the vectors and renormalizing the resultant vector, exact midpoints may not be created but that is not of concern to the algorithm. As shown in (Figure 31) the successive midpoints (1-5..) would be tested as per binary search rules and so a pixel that is valid but has one or more surrounding pixels that are invalid is converged upon. It is noted that this does not guarantee that the first crossing of the boundary is found as shown in (Figure 32).

Figure 32: Possible error with binary search

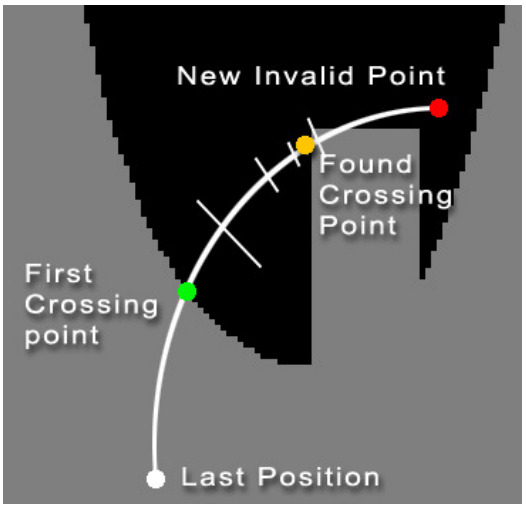

While the number of steps required for search will vary for different last and new positions I will later show that the GPU can perform such tests highly efficiently.

Concave Boundary Jumping

"A great arc connecting two points may not be fully contained in the valid region, even if the two extremities are" (Baerlocher & Boulic, 2001). This may cause an abrupt movement from a valid region to another, which are close in space but that require a long path to be connected (Baerlocher & Boulic, 2001). As suggested by Baerlocher we can minimize the effect of boundary jumping by testing the midpoint. If the midpoint is invalid the lookup of the pre-computed nearest boundary position to that mid point makes this approach highly efficient and could be repeated several times to better follow the boundary curve. If required an exhaustive pixel search could also be performed to trace the boundary between the points.

Figure 33: Avoidance of Boundary Jumping

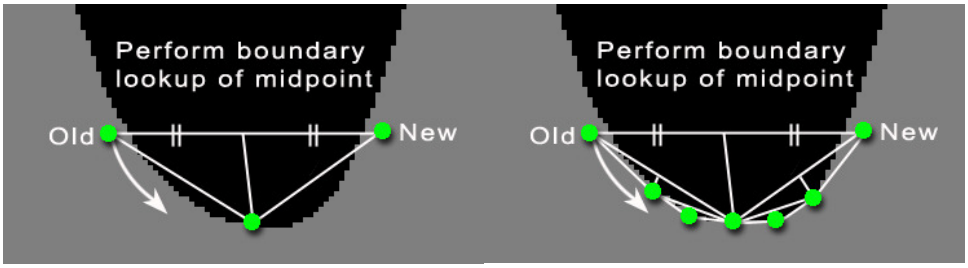

Setting Twist

An existing method to set the bone twist was possible through interaction with the y-axis of Blenders standard rotation manipulator orientated to the bone normal. However the picking of this axis with the mouse was often hindered by the presence of the other axes and so a more user friendly UI was developed (Figure 34). The other axis where removed and a partial disk was displayed indicating the angle of twist against the vertical zero twist position. This UI enabled the recording of the permissible minimum and maximum twist limit for a given swing vector either side of the zero position (each displayed in a differing shade of green). An interaction restriction of up to 180 degrees in either rotation direction was imposed. Through visual observation this was considered sufficient to capture human limits.

Figure 34: Twist setting UI

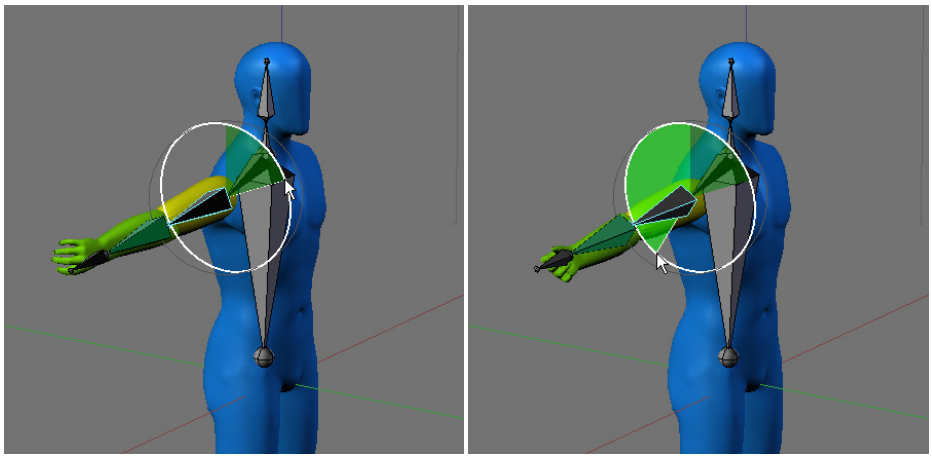

Encoding and Interpolation of Twist

Figure 35: Interpolation of Twist

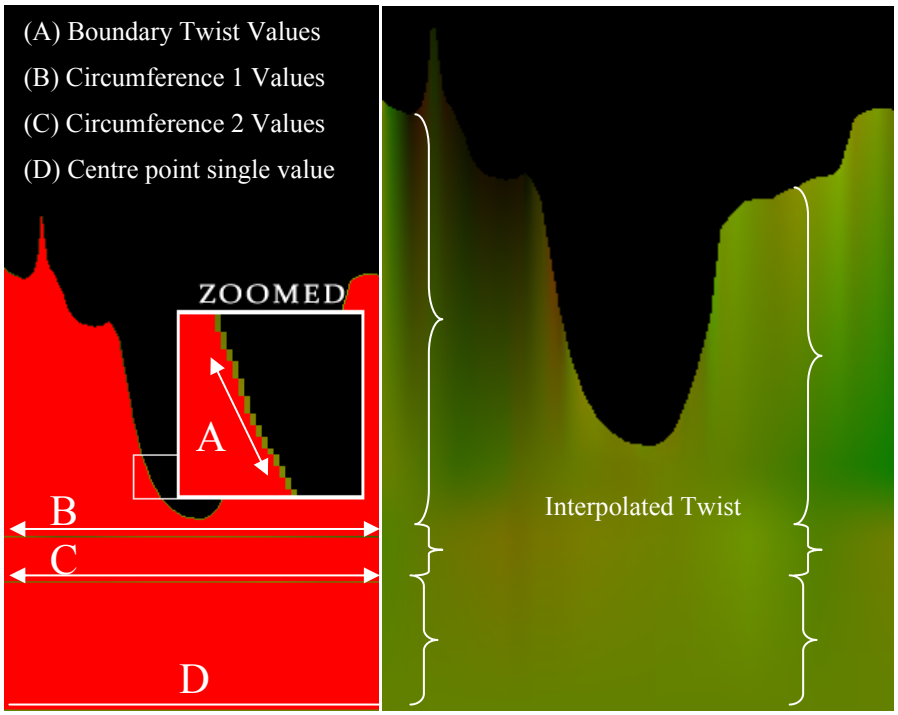

Through encoding the clockwise maximum twist for a given swing vector in the red channel (0 red being reserved) and the maximum anticlockwise twist in the green channel the lookup of a swing vector in the texture map yields the permitted twist. The values of permitted twist should be obtained from motion capture however as values for the whole discretised pixel range of swing would be laborious to obtain some form of interpolation would be desirable to fill data holes. Time constraints did not permit the scheduling of motion capture session and so as a substitute the twist freedom of my own arm at key positions were simply observed and replicated visually through use of swing and twist setting UIs. The values were then interpolated horizontally to form bands (B) and (C) as shown in (Figure 35). Similarly key twist limit points along the boundary curve were interpolated along the boundary (A) and the value of permitted twist at the initial T pose was also recorded (D). A vertical interpolation between bands was then performed followed by a 2-D convolution on the red and green channel separately to smooth the values resulting in the image to the right in (Figure 35). To save programming time this convolution was achieved in Photoshop rather than within Blender. It should be noted that their many bands could be created for greater accuracy.

Elbow shoulder Hierarchy

In certain cases to consider the range of motion of joints as independent would result in impossible poses, for example the shoulder and elbow joints could permit the hand to penetrate the chest. To capture the coupling that exists between the ranges of motion between multiple joints the following (while unimplemented) is proposed for the elbow shoulder hierarchal rotation limits. A 2-D array of the same dimensions as the joint limit text could be constructed. A further dimension would be added (Now 3-D), ranging from the maximum of any possible

anticlockwise shoulder twist through to the maximum of any possible clockwise shoulder twist at some fixed discretisation for a given swing (2-D correspondence with the texture).

The value stored at the 3-D position would be the permitted angle range for the elbow from the zero rotation of the elbow (inline with upper arm). The 3-D array is accessed by converting a given swing to its 2-D pixel coordinates as before and using the twist value of the shoulder to index to the permitted 1-D rotation value of the elbow. It is recognised that this is a very large and wasteful array structure. A lower resolution array may be sufficient such as could be achieved by scaling in half the array size in the first two dimensions. This would be indexed by diving the vector swing pixel coordinates by two and then indexing the twist value.

Figure 36: 3-D Hierarchy array

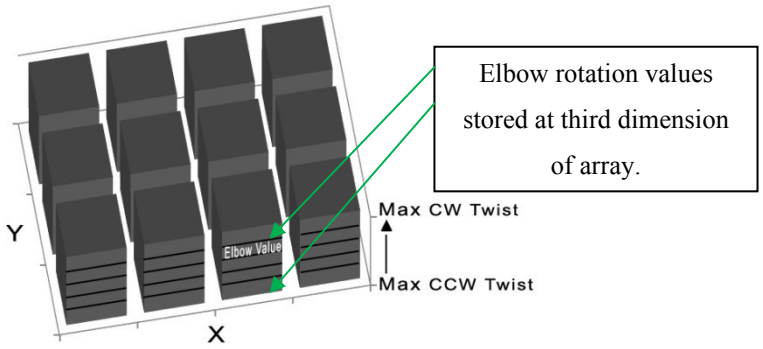

Procedure for respecting limits

- Convert the proposed orientation into its equivalent swing-twist components.
- A test is performed to determine if the swing component is within its range of motion followed by testing of twist.
- If swing is beyond its range that is first resolved through location of the closest point on the boundary curve to the proposed swing orientation. Pre-computed point is used if considered in isolation, otherwise binary search is performed.
- Twist is then resolved if beyond its limits.
- If a hierarchal elbow limit is to be respected its value is corrected to the nearest permitted value as obtained for a given shoulder swing and twist from a 3-D array.

Texture Formats

The dimensions of 256 x 512 were chosen so the image could be spit into two square images as equal power of two dimensioned textures were a format requirement for previous generations of GPUs. It is notable that if the sinus cone boundary were all that the study was concerned with then the braced range of interest shown in (Figure 23) could be contained within a single 256x256 image. Red was the chosen colour for the permissible swing region as it was considered that as red is the first entry of and RGB image it would be the quickest to index into though some image formats do in fact reverse the RGB order.

The tested joint limit texture with dimensions of 256x512 encoding swing and twist limits for a single joint has a file size of 25.3KB when using a png24 format without alpha channel. This file size is achieved because only two channels are utilised (red and green) and so compression of the blue channel is simple for the png compression technique. If a swing limiting texture were all that was required a binary image could be used.

If a stress map is desired the blue channel can be occupied by the greyscale seen in (Figure 28). The green, blue and alpha channel for pixels with a zero red value are used for indexing pre-computed boundary positions and so a 32-bit png is required (8bits per channel) (Figure 37). Pixel areas within the boundary curve do not utilise the alpha channel. The file size is 61KB. It is recognised this is still wasteful as an RGB format would be smaller, but as video game textures can often be several MBs in size optimisation was not a considered necessary. As already discussed the reason for use of the alpha channel is to aid in the indexing of the height range and therefore should the texture be split into squares of a 256x256 dimension then it would not be required.

The GPU will not process an image in png format and so a conversion is required. To support a hierarchal limit all four channels are required. An unsigned 32-bit RGBA texture in DDS format is 512KB in file size. The DXT5 format is a compressed texture format with interpolated non-pre-multiplied alpha and may offer sufficient quality at a much smaller size (128KB) but its effect on the accuracy of system has not been explored.

Figure 37: Final Joint Limit Texture

Shown with blue channel stress map within valid swing region.

Alpha channel values are not shown.

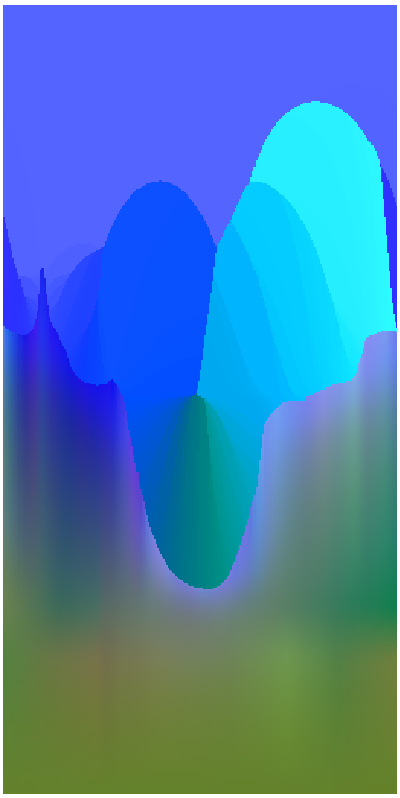

Alternative Avenue of Investigation

Research toward encoding an implicit surface to texture

The initial focus of my research was to investigate if a cube map texture could be used to encode an approximation of Herda's implicit surface to represent joint limits. It was hoped that the representation obtained from imaging Herda's 3-D surface from six directions would be sufficiently accurate at reasonable texture dimensions for the reconstruction of the surface to within a workable tolerance. An orthographic projection from each pixel of a cube face to the 3-D surface would obtain a depth value to be encoded into the colour channels of that pixel.

As already mentioned Herda's implicit surface parameterisation limits the number of primitives contributing to the iso-surface for ease of computation. If an image of the iso-surface is all that need be retained the surface can be as complex as desired.

During the manipulation of the armature bones quaternions were generated and appended to a text file. Code was written to take this list of quaternion 3-D coordinates and generate a small meta-ball for each entry of a set radius as apposed to Herda's method where meta-balls encompass multiple quaternion points. A distance measure was created to ensure quaternions already contained within a meta-ball be excluded. It was envisioned that this would largely overcome the problem of unwanted hole filling as seen in Herda's system and also not produce a largely smooth surface unless the data supported it.

It was hoped such a system would reduce Herda's surface inclusion test of a 3-D point (representing simultaneously a swing and twist) to a lookup of the corresponding pixel for each face of the cubemap. It was expected that the computation needed to yield the result would be significantly less than that for Herda's approach.

Figure 38: Visualisation of cube-map

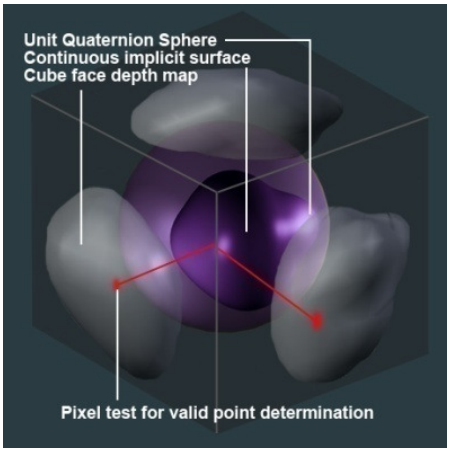

In exploration of this approach a pipeline was created within Blender to image a depth map of an implicit surface from a given camera position. Through use of this pipeline it was intended that the camera be positioned appropriately and the Cube-map be constructed from six such depth maps.

Figure 39: Depth map pipeline

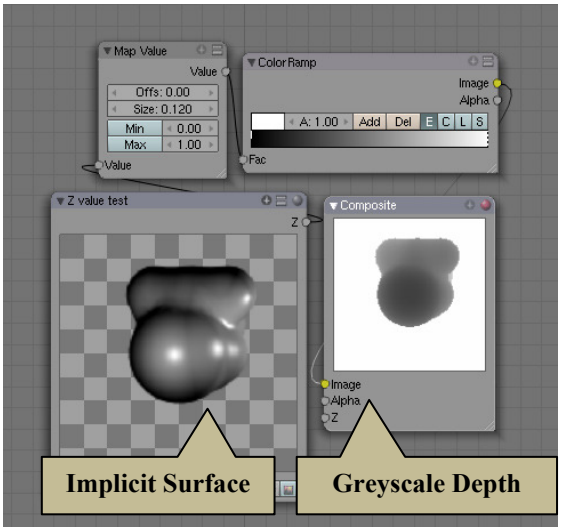

The above depth map takes no account of the internal structure of the implicit surface, only imaging its outer hull. Any caverns within the surface which denote invalid rotations must be accounted for. To do so I propose that the surface be converted to a polygon mesh as in (Figure 40). Through selection of a face on the surface of this polygon mesh all connected faces can be found and deleted. Blender has an inbuilt function for such connected face searches as seen in the menu shown in (Figure 40). This leaves only the faces not connected to outer hull and so encompass holes in the surface. A depth map of the holes can then be constructed. It was intended that the outer surface depth maps and holes depth maps be composited into different colour channels of the cube-map.

While I consider the major elements required for this approach complete, due to time constraints I had not addressed an intuitive means to edit the surface, represented hierarchal limits or resolve the boundary for points beyond limits. For these reasons I decided it would be more fruitful to pursue a more complete and user-friendly system without an implicit surface base.

Figure 40: Obtaining holes in surface

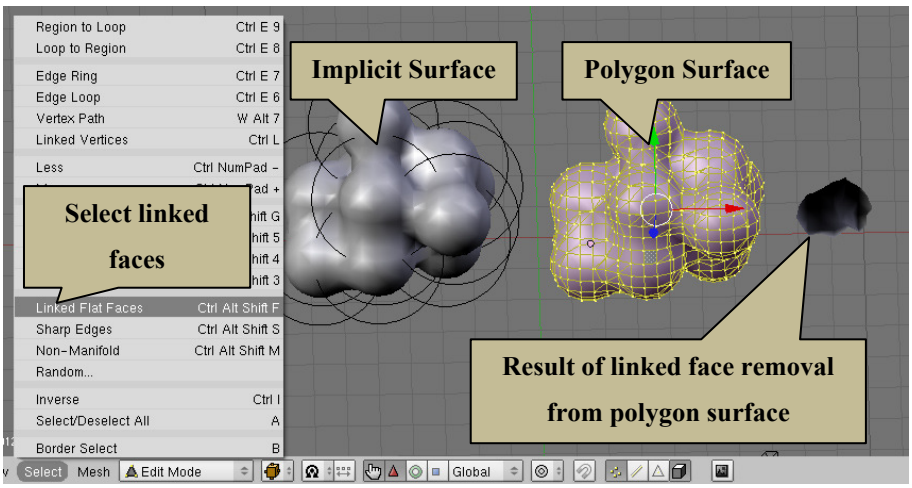

Results

Comparison of boundaries

The boundary possible through placing a minimum and maximum angle limit on each DOF as possible in Blender and other 3-D packages is visualised in (Figure 41 left) with the swing range being the carved out area of the sphere.

Figure 41: Min Max limits of each DOF vs Texture Swing Limit

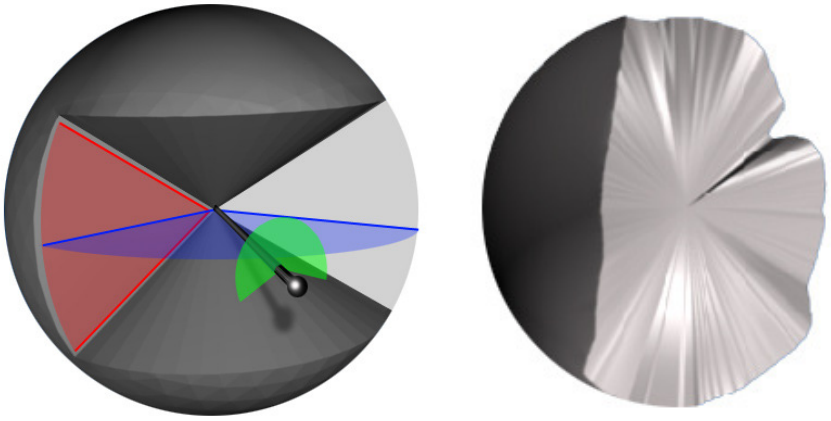

"Such a representation may be considered sufficient for mechanical simulations in general, it may not lead to realistic postures concerning the vertebrate bodies, especially the human body" (Maurel, 2000). Maurel recognises that sinus cones are a significant improvement over such a representation. Given that the proposed texture sinus boundary is at its base a different means to describe a sinus cone its properties to better describe the human range of motion similarly applies (Figure 41 right).

Execution Performance

High Level Shading Language (HLSL) is a proprietary shading language developed by Microsoft for use with the Microsoft Direct3D API. A HLSL shader was written to test the performance of the proposed algorithms for "point within boundary test" (Code 2 pg60) and "point beyond boundary correction". No impediments exist for a similar shader to be written for the OpenGl standard. The NVIDIA GeForce 6600 GT is Mid-Range GPU launched in September 2004. With a launch price of $199 it is considered a mainstream product. This GPU was chosen as a benchmark as its performance is comparable to that present in the current generation of video game console.

Profile of NVIDIA GeForce 6600 GT GPU	
Memory Interface	128-bit
Memory clock speed	1.0 GHz GDDR3
Core	500 MHz
Pipes	8

Reporting from NVIDIA FX COMPOSER 2:

FX Composer is an integrated development environment for shader authoring and provides tools for shader performance analysis across multiple GPUs. Using FX Composer the "point within bounds test" compiled with ps_3_0 requires 34 assembly instruction slots, 1 texture allocation and 33 arithmetic functions. Two registers are used. The operations completes in 15 Cycles when using FP16 precision and 16 Cycles at FP32 precision. 15-16 Cycles is a very minimal amount of processing and once the texture is loaded into the GPU memory communication with the CPU would be minimal in this system. A more experienced shader programmer would also likely be able to optimise the shader for enhanced performance.

Table 1: Boolean Test Shader Simulated Results

GPU	Driver	Type	Cycles	Registers
GeForce 6600 GT*	163.2	fragment	15	2
GeForce 6800	163.2	fragment	15	2
GeForce 6800 GT	163.2	fragment	15	2
GeForce 6800 Ultra	163.2	fragment	15	2
GeForce 7800 GT Released (August , 2005)	163.2	fragment	11	3
*Benchmark GPU				

With a cycle rate of five hundred million per second and an assumed 60 tests for the shoulder joint per second (60 fps animation) then under ideal circumstances a single test would theoretically utilise less than 0.000002% of the GPU execution budget. While a simplification of the nature of GPU processing this figure indicates how minimal the impact of such tests on an execution budget are and so are deemed suitable for real time applications. The "point beyond boundary correction" for a vector considered in isolation is also calculable in a fixed low number of cycles. 24 Cycles for execution on the GeForce 6600 GT, 65 instruction slots used (1 texture, 64 arithmetic).

Table 2: Corrective Shader Simulated Results

GPU	Driver	Type	Cycles	Registers
GeForce 6600 GT*	163.2	fragment	24	4
GeForce 6800	163.2	fragment	24	4
GeForce 6800 GT	163.2	fragment	24	4
GeForce 6800 Ultra	163.2	fragment	24	4
GeForce 7800 GT Released (August , 2005)	163.2	fragment	16	4
*Benchmark GPU				

The number of cycles required for a "point beyond boundary correction" with consideration of a known previous valid vector is not fixed however its worst case could be calculated given that the largest distance the binary search could possibly need to cover is the diagonal of the joint limit texture: $\sqrt{256^2 + 512^2}$.

Recommendations for Further Work

Improvement to User Interface

The user interface of the tool consists of a large number of buttons many of which were simply of use in debugging the system. A through review of the UI is required to make it more user friendly. For users uninterested in editing limits I propose that a library of pre-generated joint limit textures be accessible.

Acceptance of the system into blender package

The development of the system required modification to a large number of diverse systems within blender. Due to a lack of what I would consider sufficient development documentation, a lack of knowledge of Blenders intended development route and my unfamiliarity with the C coding language many coding hacks were involved in the creation of this system. Updates to the structure of the blender code base is expected in the forthcoming 2.5 release and so any new additions must respect these changes. For these reasons a rewrite of my code is necessitated and the system will not be submitted for consideration of inclusion within Blender in its current form. However the Blender development and user communities have reacted most favourably to the features proposed and eager to see their continued development and inclusion within Blender.

Implementation of Hierarchal limits and IK integration

The coding of hierarchal limits and the integration of system into IK evaluation remains undone. While not considered difficult to code, implementation of these features would greatly enhance the usefulness of the system.

Mip-mapping

There may exist situations where texture memory allocation is of concern. Mipmaps would present a means to balance this issue with accuracy of result. This could be leveraged in simulations of large crowds of characters where if each were to have unique joint limits (perhaps due to their armament) a characters distance from the camera could determine the required mipmap level. This would provide a courser but more efficient lookup for distant characters.

Continued investigation of a cube mapped implicit surface

Cubemaps are commonly used in modern computer graphics and their use is often optimised on GPU hardware (Appendix pg.55). The quantisation of a continuous surface to pixels even at high texture resolutions would result in some inaccuracies. While I did not address this and several other issues such as a means to designate hierarchal limits, the cubemap appears in principle a promising representation and I believe warrants further research.

Conclusion

The proposed system addresses many of features which I consider desirable for a joint limit system.

Accuracy of result and a convenient means of limit storage

While the limits have been discretised the resolution obtained is considered sufficient for many applications. The texture is constructed such that the singularity of axis angle parameterisation is far from the sinus boundary. A texture format for data such as normal maps is widely used in the video games industry and is so a familiar and convenient storage mechanism.

Need for variance from generic constraints

The proposed UI enhancements and pixel painting tools provide a convenient means to edit a sinus boundary.

Address lack of tools

The system was developed within a popular free 3-D package and many of its features are expected to be adopted in a public release of that software.

Joint Coupling

A 3-D array appears to be suited to capture the relationship between shoulder and elbow and could be similarly applied to the hip and knee.

Limit avoidance and stress measurement

A stress gradient map is easily integrated into the texture format.

Requirement for real-time evaluation and resolution of limits

It is in this area that the proposed system excels as it the GPU can be utilised in the evaluation and resolution of limits. While timing information is absent from much of the existing research from consideration of the operations other methods require I am confident that the proposed system outperforms them by many orders of magnitude.

I have described a method of limiting joint motion based on a texture based approximation to a sinus cone for joints with three rotational degrees of freedom. The system addresses a means to encode permitted twist at the level of discretisation of swing. The system provides a more realistic range of motion than simple limits on Euler angles. Run time calculations are performable on the GPU and are suited to real-time evaluation. The system developed is considered to be of significant use to simulations utilising dynamics, AI or physical motion generation.

YouTube Videos of System in Operation

http://www.youtube.com/watch?v=GWAmw6Ycu8I&fmt=18

http://www.youtube.com/watch?v=QUmFYtWTmxA&fmt=18

Bibliography

Aubel, A., & Thalmann, D. (2000). Efficient Muscle Shape Deformation. *IFIP Conference Proceedings; Vol. 196The Netherlands* (pp. 132 - 142). Deventer, The Netherlands: Kluwer, B.V.

Baerlocher, P., & Boulic, R. (2001). Parametrization and range of motion of the ball-and-socket joint. *Deformable Avatars* (pp. 180-190). Lausanne: Kluwer Academic Publishers.

Bittar, E. T., Tsingos, N., & Gascuel, M.-p. (1995). Automatic reconstruction of unstructured 3D data: Combining medial axis and implicit surfaces. *Computer Graphics Forum* , 14(3):457-468.

Bourke, P. (1987, November). *Determining if a point lies on the interior of a polygon.* Retrieved 08 17, 2008, from The University of Western Australia: http://local.wasp.uwa.edu.au/~pbourke/geometry/insidepoly/

Craig, J. J. (1989). *Introduction to Robotics: Mechanics and Control.* Upper Saddle River, NJ: Pearson/Prentice Hall.

Engin, A., & Tümer, S. (1989). Three-dimensional kinematic modeling of the human shoulder complex. *Journal of Biomechanical Engineering* , 107-121.

Grassia, S. F. (1998). Practical parameterization of rotations using the Exponential Map. *Journal of Graphics Tools, 3(3)* , 29-48.

Guillard, G., & Magnenat-Thalman, N. (2007). Ball-and-socket joint motion description using spherical medial representation. *International Conference of the IEEE EMBS Cite Internationale* (pp. 23-26). Lyon: IEEE Computer Society Press.

Hanson, A. J. (1998). Constrained optimal framings of curves and surfaces using quaternion gauss maps. *Visualization* (pp. 375-382). NC: IEEE Computer Society Press.

Herda, L., Urtasun, R., & Fua, P. (2003). Automatic Determination of Joint Limits using Quaternion Field Boundaries. *In International Journal for Robotis Research, vol.22, no. 6* , 419-436.

Herda, L., Urtasun, R., & Fua, P. (2005). Hierarchical Implicit Surface Joint Limits for Human Body Tracking. *Computer Vision and Image Understanding Volume 99 , Issue 2* , 189 - 209.

Hodgins, J. K., O'Brien, J. F., & Tumblin, J. (1998). Perception of human motion with different geometric models. *IEEE Transactions on Visualization and Computer Graphics 4* , 307-316.

Jing, H., & Prakash, E. C. (2000). SinusCone - A ThetaPhi Algorithm for Human Arm Animation. *Proceedings of the International Conference on Information Visualisation* (p. 318). London, England: IEEE Computer Society Washington, DC, USA.

Kavan, L. (2008). Geometric Skinning with Approximate Dual Quaternion Blending. *ACM Transactions on Graphics* .

Korein, J. U. (1985). *A Geometric Investigation of Reach.* Cambridge: The MIT Press.

Lee, S.-H., & Terzopoulos, D. (2008). Spline Joints for Multibody Dynamics. *ACM Transactions on Graphics.* New York: ACM.

Liu, Q., & Prakash, E. (2003). The Parameterization of Joint Rotation with the Unit Quaternion. *VIIth Digital Image Computing: Techniques and Applications* (pp. 409-418). Sindey: CSIRO Publishing.

Maurel, W. (2000). Human Upper Limb Modeling including Scapulo-Thoracic Constraint and Joint Sinus Cones. *Computers & Graphics, Pergamon Press, 24(2)* , 203 - 218.

Ramamoorthi, R., & Barr, A. H. (1997). Fast Construction of Accurate Quaternion Splines. *International Conference on Computer Graphics and Interactive Techniques* (pp. 287 - 292). Los Angeles: ACM Press.

Schmidt, J., & Niemann, H. (2001). Using Quaternions for Parametrizing 3–D Rotations in Unconstrained Nonlinear Optimization. *Vision, Modeling,and Visualization 2001* (pp. 399–406). Stuttgart, Germany: AKA/IOS Press, Berlin.

Shao, W., & Ng-Thow-Hing, V. (2003). A General Joint Component Framework for Realistic Articulation in Human Characters. *Symposium on Interactive 3D graphics* (pp. 11-18). Monterey, California: ACM New York.

Shoemake, K. (1985). Animating rotation with quaternion curves. *Computer Graphics SIGGRAPH 1985 volume 19* (pp. 245-254). San Francisco: ACM press.

Tolani, D., Badler, N., & Gallier, J. (2000). *A kinematic model of the human arm using triangular b'ezier spline surfaces.*

Wang, X., Maurin, M., Mazet, F., De Castro Maia, N., Voinot, K., Verriest, J., et al. (1998). Three-dimensional modelling of the motion range of axial rotation of the upper arm. *Journal of Biomechanics 31(10)* , 899-908.

Wilhelms, G. (2001). Fast and Easy Reach-Cone Joint Limits. *Journal of Graphics Tools (6)2* , 27–41.

Wrotek, P., Jenkins, O. C., & McGuire, M. (2006). Dynamo: dynamic, data-driven character control with adjustable balance. *Proceedings of the 2006 ACM SIGGRAPH symposium on Videogames* (pp. 61-70). Boston, Massachusetts: ACM New York, NY, USA.

Zhao, J., & Badler, N. (1989). *Real time inverse kinematics with joint limits and spatial constraints.* University of Pennsylvania: Technical Report MS-CIS-89-09, Department of Computer and Information Science.

Appendix

Figure 42: Complete UI

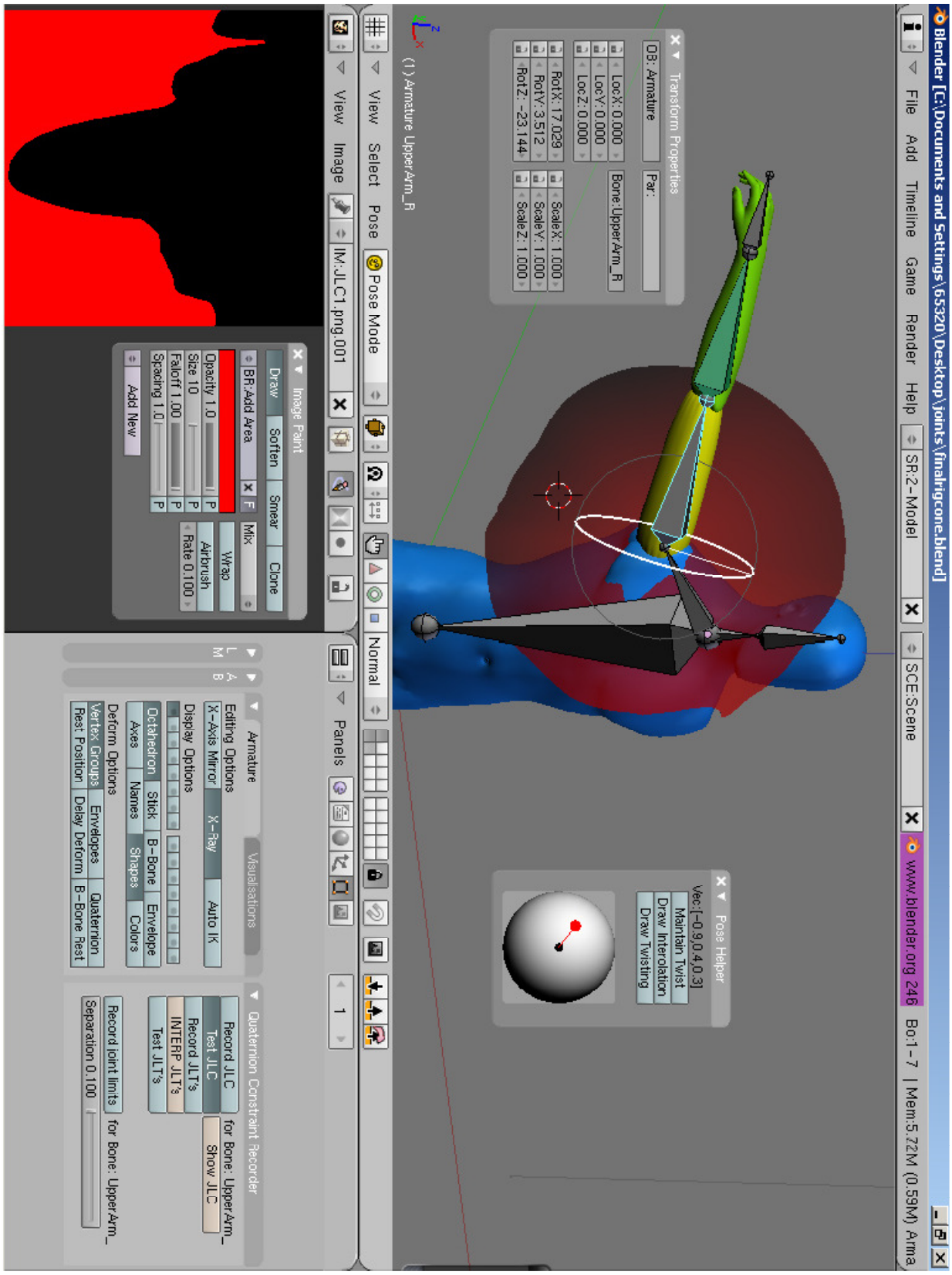

The anatomical structure of the shoulder complex

Figure 43: The left shoulder

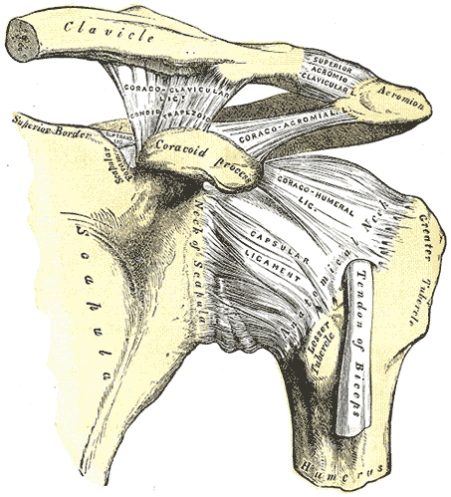

Acromioclavicular joints, & the proper ligaments of the scapula

Complex nature of shoulder

This image is in the public domain because its copyright has expired.

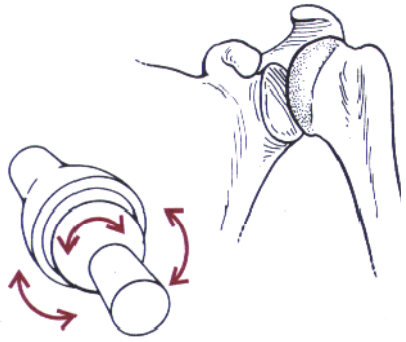

Simplification to a ball and socket joint

Reproduced from Biomechanical Basis of Human Movement by Joseph Hamill and Katheen M. Knutzen, Williams & Wilkins 1995, ISBN: 0-683-03863-X

The use of texture lookups in the graphics field

Modern graphics processing units (GPUs) expose many of the same operations supported by CPUs through parallel programmable shaders. As computations involved in the processing of 3D graphics (the primary function of a GPU) make extensive use of matrix and vector operations other applications reliant on such structures may be suited to GPU rather than CPU execution. The GPU is increasingly being used for more general purpose non-graphical calculations.

A commonly used means to map and stream data to the GPU for such applications is a two dimension grid of values. This fits naturally with the traditional texture rendering model supported by the GPU. The GPU memory holds these data textures and provides means for their access. Textures with up to four channels each with an 8-bit range are widely supported with more recent cards exceeding this range. 32-bit floating point textures have recently been accepted to the Direct X and OpenGL formal specifications. In recent years textures of non power of two dimensions have been permitted on GPUs however for backward compatibly this restriction is often still respected.

Figure 44: Conversions and Modify menu

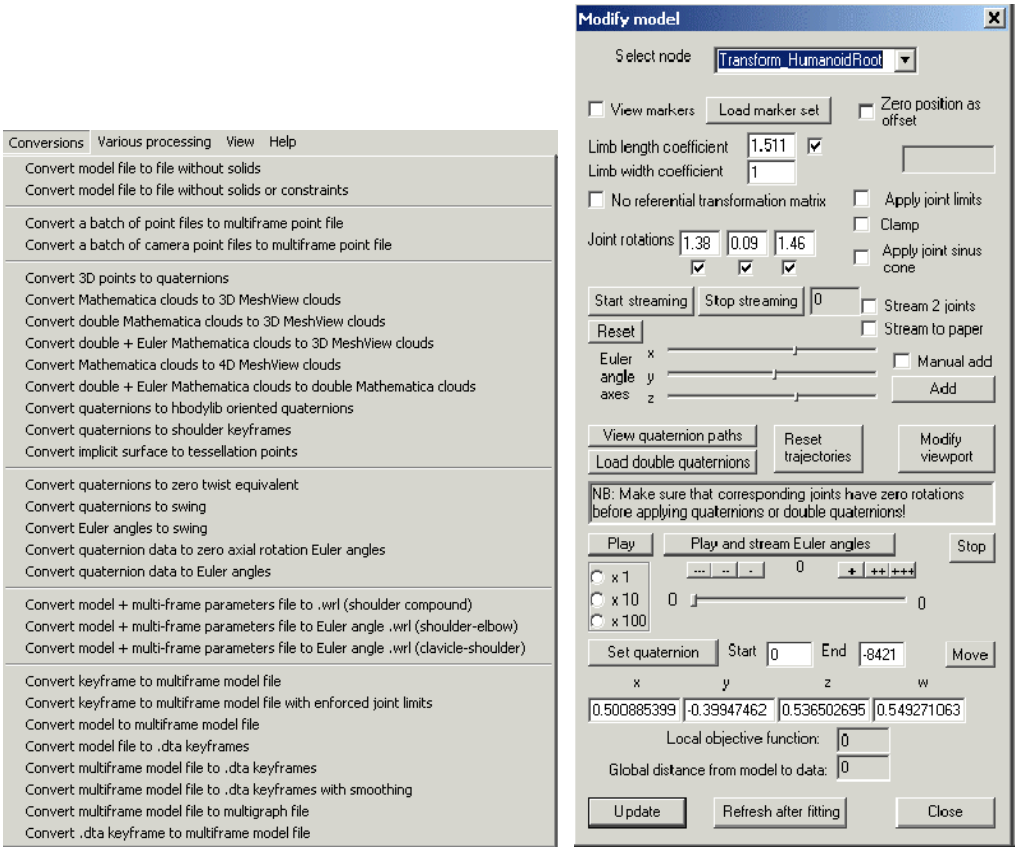

Existing UIs within popular 3-D suites

A shown in screen shots below many 3D packages use a virtual sphere rotation manipulator as shown in (Figure 45). Within Blender clicking and dragging the virtual sphere on the non axial lines does not have the same intuitive behaviour as in Maya or 3D Studio Max and so this interface issue was addressed in the tool created.

Figure 45: Common virtual sphere rotation manipulator

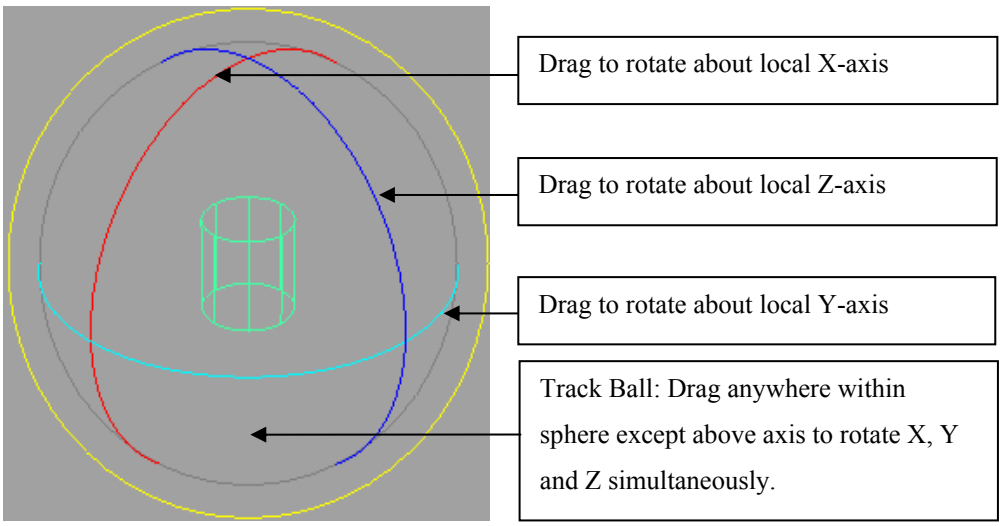

Maya

Figure 46: Euler Angle Constraints

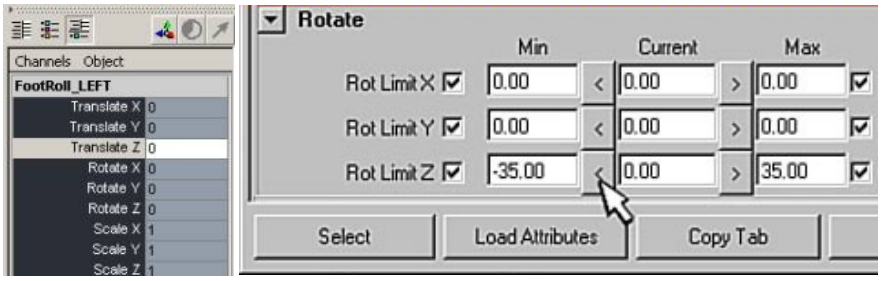

3D Studio Max

Figure 47: Euler Angle Constraints

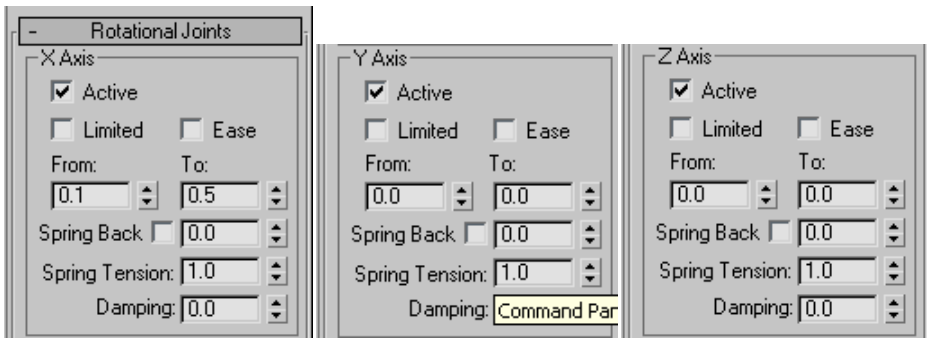

Figure 48: Virtual Sphere Rotation Manipulator with track ball control

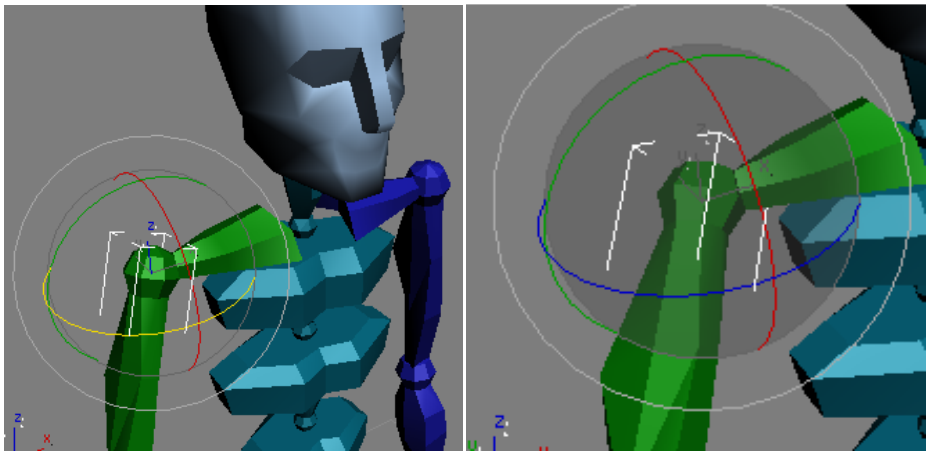

Blender (without proposed modification)

Figure 49: Blender UI

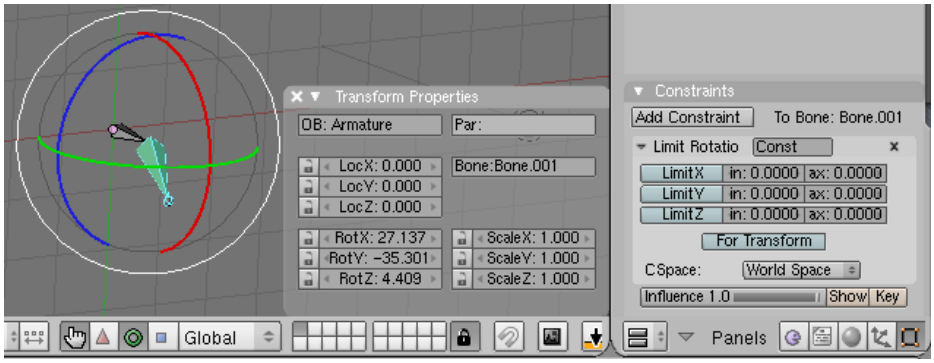

Left: Rotation Manipulator, Middle: Axis locking, Right: Euler Angle Constraints

XSI

Figure 50: XSI UI

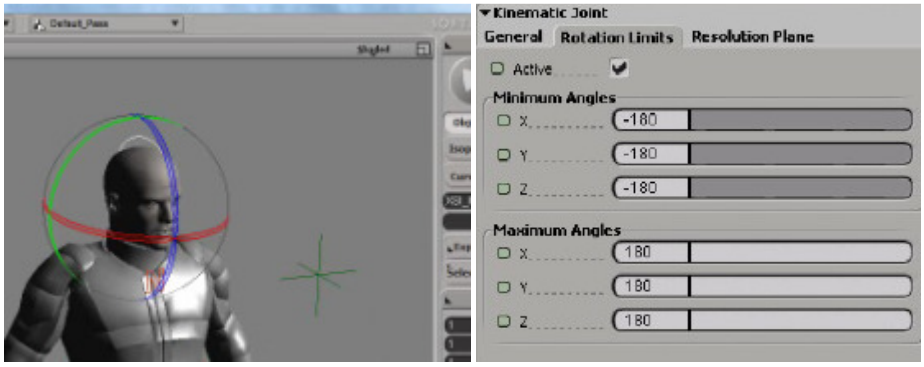

Left: Virtual Sphere Rotation Manipulator with track ball control, Right: Euler Angle parameters

---

Figure 51: Video game character rig

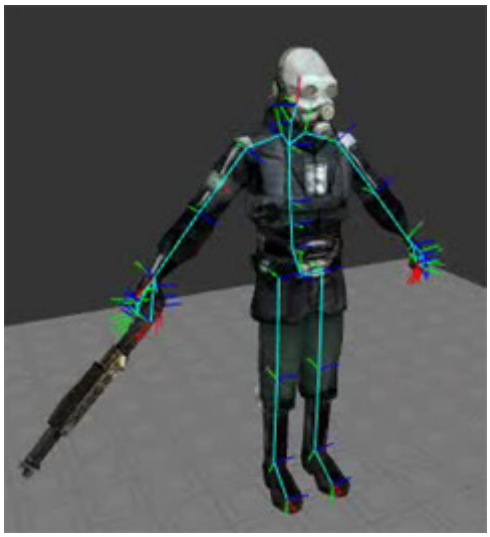

Figure 52: Two spherical polygons define a complex admissible spherical region.
Reprinted from (Baerlocher & Boulic, 2001)

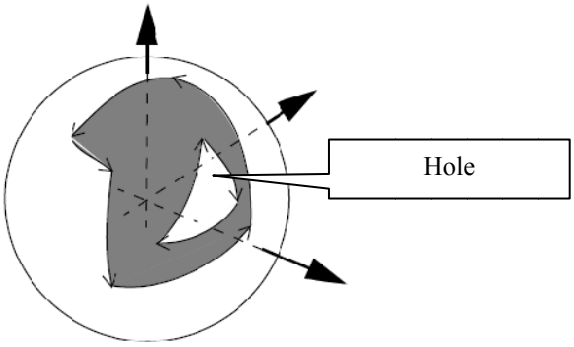

Figure 53: Throughput of the simulated GPU's measured in Mega Pixels per Second

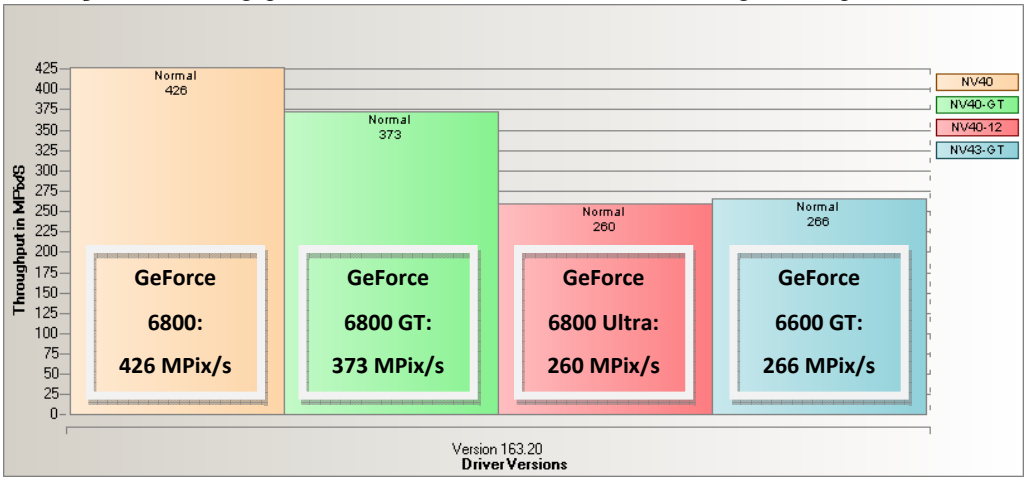

Code Snippits

Code 1: Conversion from Vector & Rotation to Quaternion (Present in Blender)

```
void VecRotToQuat( float *vec, float phi, float *quat)
{
	/* rotation of phi radials around vec */
	float si;

	quat[1]= vec[0];
	quat[2]= vec[1];
	quat[3]= vec[2];

	if( Normalize(quat+1) == 0.0) {
		QuatOne(quat);
	}
	else {
		quat[0]= (float)cos( phi/2.0 );
		si= (float)sin( phi/2.0 );
		quat[1] *= si;
		quat[2] *= si;
		quat[3] *= si;
	}
}
```

Shader HLSL Code 1

Code 2: Shader for "Point within boundary" test

```
float3 testVector;

texture limitMap <
string ResourceName="FINALJLC.png";
string ResourceType = "2D";
string UIName="Joint Limit Texture";
>;

sampler texSampler = sampler_state
{
    Texture   = <limitMap>;
    MipFilter = LINEAR;
    MinFilter = LINEAR;
    MagFilter = LINEAR;
    AddressU  = Clamp;
    AddressV  = Clamp;
};

float4 LimitPS(): COLOR
{
    const float PI2=6.28318531;
    const float widthDivideByPI2=40.5845104;

    float2 xy;

    float theta = atan2(testVector[1],testVector[0]);
            if(theta<0) { theta += PI2; }

    xy[0]=theta*widthDivideByPI2;
    xy[1] = (sqrt(testVector[0]*testVector[0] +
testVector[1]*testVector[1])*255);

    float4 colour=tex2D(texSampler,xy);
    float4 answer;
    if (colour[0]==0)
    {
        //THEN INVALID
        answer=float4(0,0,0,1);

    }else
    {
        //Valid
        answer=float4(0,0,0,-1);
    }
    return answer;
}

technique technique0
{
    pass p0
    {
        PixelShader = compile ps_3_0 LimitPS();
    }
}
```

Shader Assembly 1

Code 3: Assembly Code of above shader

```
// Generated by Microsoft (R) D3DX9 Shader Compiler
9.12.589.0000
//
// Parameters:
//   float3 testVector;
//   sampler2D texSampler;
//
// Registers:
//   Name         Reg   Size
//   ------------ ----- ----
//   testVector   c0       1
//   texSampler   s0       1
//
// Default values:
//   testVector
//     c0   = { 0, 0, 0, 0 };

    ps_3_0
    def c1, 0.999866009, 0, 1, -3.14159274
    def c2, 0.0208350997, -0.0851330012, 0.180141002, -
0.330299497
    def c3, -2, 1.57079637, 6.28318548, 40.5845108
    def c4, 255, 1, -1, 0
    dcl_2d s0
    abs r1.xy, c0.yxzw
    add r0.xy, -r1.yxzw, r1
    cmp r1.xy, r0.x, r1.yxzw, r1
    rcp r0.w, r1.y
    mul r0.w, r1.x, r0.w
    mul r0.z, r0.w, r0.w
    mad r0.x, r0.z, c2.x, c2.y
    mad r0.x, r0.z, r0.x, c2.z
    mad r0.x, r0.z, r0.x, c2.w
    mad r0.z, r0.z, r0.x, c1.x
    mul r0.x, r0.w, r0.z
    cmp r0.z, r0.y, c1.y, c1.z
    mad r0.w, r0.x, c3.x, c3.y
    mad r0.x, r0.w, r0.z, r0.x
    add r1.w, -c0.x, c0.y
    mov r0.yz, c1
    cmp r0.w, c0.x, r0.y, r0.z
    cmp r1.xy, r1.w, c0, c0.yxzw
    mad r0.x, r0.w, c1.w, r0.x
    cmp r1.xy, r1, c1.yzzw, c1.zyzw
    add r0.z, r0.x, r0.x
    mul r0.w, r1.y, r1.x
    mad r0.z, r0.w, -r0.z, r0.x
    dp2add r0.w, c0, c0, r0.y
    add r0.y, r0.z, c3.z
    rsq r0.w, r0.w
    cmp r0.z, r0.z, r0.z, r0.y
    rcp r0.w, r0.w
    mul r0.x, r0.z, c3.w
    mul r0.y, r0.w, c4.x
    texld r0, r0, s0
    cmp oC0.w, -r0_abs.x, c4.y, c4.z
    mov oC0.xyz, c1.y
```

Shader HLSL Code 2

Code 4: Shader for "Correction of point beyond bounds"

```
float3 testVector;

texture limitMap <
string ResourceName="FINALJLC.png";
string ResourceType = "2D";
string UIName="Joint Limit Texture";
>;

sampler texSampler = sampler_state
{
    Texture   = <limitMap>;
    MipFilter = LINEAR;
    MinFilter = LINEAR;
    MagFilter = LINEAR;
    AddressU  = Clamp;
    AddressV  = Clamp;
};

float4 LimitPS(): COLOR
{
    const float PI2=6.28318531;
    const float widthDivideByPI2=40.5845104;

    float2 xy;
    float recoveredRadius;

    float theta = atan2(testVector[1],testVector[0]);
    if(theta<0) { theta += PI2; }

    xy[0]=theta*widthDivideByPI2;
    xy[1] = (sqrt(testVector[0]*testVector[0] +
testVector[1]*testVector[1])*255);

    float4 colour=tex2D(texSampler,xy);
    float4 answer;

    if (colour[0]==0)
    {
        //THEN INVALID
        //CORRECT
        xy[0]=colour[1];
        xy[1]=colour[2]+(255-colour[3]);

        theta=(xy[0]*PI2/255.0);

      if (xy[1]>255)
      {
          xy[1]=511-xy[1];
          recoveredRadius=xy[1]/255.0;
          answer[2]=-(sqrt(1.0-
(recoveredRadius*recoveredRadius)));
      }
      else
      {
          recoveredRadius=xy[1]/255;
          answer[2]=sqrt(1.0-
(recoveredRadius*recoveredRadius));
      }

      answer[0]=(cos(theta))*recoveredRadius;
```

```
      answer[1]=(sin(theta))*recoveredRadius;

    }else
    {
        //Valid
        answer=float4(0,0,0,-1);
    }
    return answer;
}

technique technique0
{
    pass p0
    {
        PixelShader = compile ps_3_0 LimitPS();
    }
}
```

Shader Assembly 2

Code 5: Assembly Code of above shader

```
////////////////////////////////////////////////////////////
//
// Technique: technique0
// Pass: p0
////////////////////////////////////////////////////////////
//
//
// Generated by Microsoft (R) D3DX9 Shader Compiler
9.12.589.0000
//
// Parameters:
//
//   float3 testVector;
//   sampler2D texSampler;
//
//
// Registers:
//
//   Name         Reg   Size
//   ------------ ----- ----
//   testVector   c0       1
//   texSampler   s0       1
//
//
// Default values:
//
//   testVector
//     c0   = { 0, 0, 0, 0 };
//

    ps_3_0
    def c1, 0.999866009, 0, 1, -3.14159274
    def c2, 0.0208350997, -0.0851330012, 0.180141002, -
0.330299497
    def c3, -2, 1.57079637, 6.28318548, 40.5845108
    def c4, 255, 511, 0.00392156886, 0
    def c5, 0.00392156839, 0.5, 6.28318548, -3.14159274
    dcl_2d s0
    abs r1.xy, c0.yxzw
    add r0.xy, -r1.yxzw, r1
```

```
    cmp r1.xy, r0.x, r1.yxzw, r1
    rcp r0.w, r1.y
    mul r0.w, r1.x, r0.w
    mul r0.z, r0.w, r0.w
    mad r0.x, r0.z, c2.x, c2.y
    mad r0.x, r0.z, r0.x, c2.z
    mad r0.x, r0.z, r0.x, c2.w
    mad r0.z, r0.z, r0.x, c1.x
    mul r0.x, r0.w, r0.z
    cmp r0.z, r0.y, c1.y, c1.z
    mad r0.w, r0.x, c3.x, c3.y
    mad r0.x, r0.w, r0.z, r0.x
    add r1.w, -c0.x, c0.y
    mov r0.yz, c1
    cmp r0.w, c0.x, r0.y, r0.z
    cmp r1.xy, r1.w, c0, c0.yxzw
    mad r0.x, r0.w, c1.w, r0.x
    cmp r1.xy, r1, c1.yzzw, c1.zyzw
    mul r0.w, r1.y, r1.x
    add r0.z, r0.x, r0.x
    mad r0.z, r0.w, -r0.z, r0.x
    dp2add r0.w, c0, c0, r0.y
    add r0.y, r0.z, c3.z
    rsq r0.w, r0.w
    cmp r0.z, r0.z, r0.z, r0.y
    rcp r0.w, r0.w
    mul r0.x, r0.z, c3.w
    mul r0.y, r0.w, c4.x
    texld r0, r0, s0
    cmp r0.x, -r0_abs.x, c1.z, c1.y
    if_ne r0.x, -r0.x
      add r0.w, -r0.w, r0.z
      add r0.w, r0.w, c4.x
      mad r0.z, r0.y, c5.x, c5.y
      frc r0.z, r0.z
      add r0.xy, -r0.w, c4
      mad r1.w, r0.z, c5.z, c5.w
      mul r2.x, r0.y, c4.z
      mul r1.x, r0.w, c4.z
      mad r0.z, r2.x, -r2.x, c1.z
      mad r0.w, r1.x, -r1.x, c1.z
      rsq r0.z, r0.z
      rsq r0.w, r0.w
      rcp r2.y, r0.z
      rcp r1.y, r0.w
      mov r2.y, -r2.y
      cmp r1.xy, r0.x, r1, r2
      sincos r0.xy, r1.w
      mul oC0.xy, r1.x, r0
      mul oC0.zw, r1.y, c1.xyzy
    else
      mov oC0, -c1.yyyz
    endif

// approximately 65 instruction slots used (1 texture, 64
arithmetic)
```